5-8-2004

Giant Magnetoresistance in Magnetic Multilayers Using a New Embossed Surface

Athanasios Chalastaras
University of New Orleans

GIANT MAGNETORESISTANCE IN MAGNETIC MULTILAYERS USING A NEW EMBOSSED SURFACE

A Thesis

Submitted to the Graduate Faculty of the
University of New Orleans
in partial fulfillment of the
the requirements for the degree of

Master of Science

in

The Department of Physics

by

Athanasios Chalastaras

B.S., University of New Orleans, 2001

August 2004

DEDICATION

This work is dedicated to the memory of my beloved little brother Panayiotis Chalastaras who gracefully touched our lives. We will never forget you.

ACKNOWLEDGMENTS

I would like to thank to the highest degree my family and all their unconditional support they have given me throughout my life. My father Ioannis, my mother Panayiota, my older brother Demitrios, and younger one Spyridon have been there for me with immense encouragement and loyal devotion. This work would not be possible without their mental and emotional contributions.

I am greatly thankful to my supervisor professor Leszek Malkinski who taught me with a wealth of knowledge and unlimited patience. This project could not have been completed without his inspiring guidance. Professor Carl Ventrice has been an excellent support throughout my years at the department of Physics at UNO. His efforts and encouragement made it possible for me to start studying my favorite subject.

I would also like to thank my colleagues Dr. Andiry Vovk for his support and valuable opinions and Dr. Volodymyr Golub with his help with PPMS measurements. My many thanks to my collaborators form South Korea for their supply of embossed surfaces Jin-Seung Jung, Seung-Lim Oh, and Jin-Kyu Lee.

Professor JinkeTang's opinions have been greatly respected, professor Kevin Stokes' suggestions were of enormous aid, professor Gregory Seab's discussions were always searching, professor George Ioup's joyful debates have been inspiring, professor Ashok Puri's help with

the graduate coordination has been a true problem solver, and professor Joseph Murphy's recommendations were superb. Ms. Sandra Merz has been an excellent source of courage and friendship during my physics studies at UNO. She is a true problem solver and of great assistance at this department. Mr. N. B. Day has been of a great assistance during my teaching experience.

I would like to thank Simella Tsaloukidou for her limitless assistance and intellectual inspiration. She has been a true friend and a believer in my dreams.

Mariella Gastanaduy has shown me important things in my life that I was oblivious to concede. Her inexhaustible friendship has been a valuable aid to my education.

TABLE OF CONTENTS

LIST OF FIGURES

ABSTRACT

Previous research on new novel substrates for giant magnoresistance structures has indicated that a net increase in the effect is present. The substrates studied were V-grooved or stepped, however research presented in this thesis used an embossed surface manufactured from alumina oxide which consisted of regular hexagonal arrays with spacing of 110 nm and pore diameter of 60 nm. The physical properties measurements unveiled a net enhancement of the giant magnetoresistance effect thru the whole range of the copper spacer thicknesses deposited with direct current magnetron sputter. The maximum net increase appeared for a spacer thickness of 4.0 nm where the flat silicon substrate yielded a 3 % increase but the embossed surface substrate generated a 12% increase with an overall effect of a 4-fold net enhancement of the effect. Both the aluminum oxide substrates and the thin films structures can be manufactured inexpensively and can be also mass-produced, which are welcoming advantages for the technology sector of magnetic sensing.

CHAPTER 1

Introduction

The characteristics of metallic multilayers and their magnetic properties have propelled the field of magnetoelectronics in a key position as technology advances. As the technology scale shrinks to the nanoscale, the effects of the electric transport through the magnetic materials become of great significance. The spin of the charge carriers (i.e., electrons) also becomes important due to the fact that they give rise to the magnetism in solids by means of magnetic moments. The influence of the spin on the magnetic transport of the electrons is the basic idea behind the vast research and industrial fields called magnetoelectronics [1].

Giant magnetoresistance (GMR) is definitely one of the most influential phenomena in the magnetoelectronics area. It is the change in magnetoresistance (MR) in an artificial multilayer structure [14] that is consisted from thin metallic non-ferromagnetic and ferromagnetic layers (or granular systems [13] not discussed in this thesis). This net change in resistance happens over a small magnetic field range and is substantial at room temperature. These two main advantages make the GMR effect a very good candidate for magnetic field sensing applications. Furthermore, low manufacturing and implementing costs of GMR sensors yield an enormous applicability domain that has surpassed the

expectations of even the more optimistic scientists. However, the vastly hungry-for-higher-density of bytes per unit area society enforces the scientific community to look for ways to improve or even replace the current GMR sensing technology. This work is dedicated to achieving the first part: improving the GMR sensors. This choice was not an easy task since the question of limitations of the technology in question had to be addressed in a priority manner. The step of searching for appropriate ways to advance the field was on the table once the decision that the GMR technology had the required foundation for further improvement. One of the most obvious ways to achieve the set goal mentioned above was to search for interfaces between the magnetic and non-magnetic layers. Some research had been done in the field about the orientation and surface effects [7], but no research was found in completely changing the surface geometry to regular hexagonal pattern. The embossed surface chosen was shown to justify our initial perception of improving the GMR effect.

CHAPTER 2

Giant Magnetoresistance Phenomenon

2.1 History

GMR is the change of resistance of special structures when a magnetic field is applied. It was first observed in multilayers 1988 [2, 14] by Baibich *et al* using Iron/Chromium (Fe/Cr) multilayers and by Binasch *et al*. The granular GMR effect (not discussed in this project) was also discovered in the 1990s [14]. The observation of the multilayer GMR effect showed a change in the magnetoresistance (MR) of 50% at 4.2 Kelvin (K), an order of magnitude increase form previous results as reported by Baibich [2,3]. This change in magnetoresistance was noted against any previous MR observations. Baibich observed in Iron/Chromium (Fe/Cr) multilayers a dramatic change in magnetoresistance (MR). A graph of Baibich's original observations is shown in figure 2.1. On the left part of figure 2.1, the hysteresis loops for three different structures of Fr/Cr multilayers is observed at 4.2 K. The magnetic field responsible for saturation of the magnetoresistance is about 20 kOe depending on the spacer thickness and the number of multilayer repetitions. Moreover, the antiferromagnetic coupling is a function of the thickness (angstroms, Å) of the Cr spacer, which is evident in the same figure. The right graph of the same figure shows the relative change in resistance as a function of the external magnetic field.

The spacer between the magnetic layer and its thickness is probably one of the most important parameters in GMR structures. Again, the importance of the Cr spacer is evident and will be discussed in more detail further in this paper.

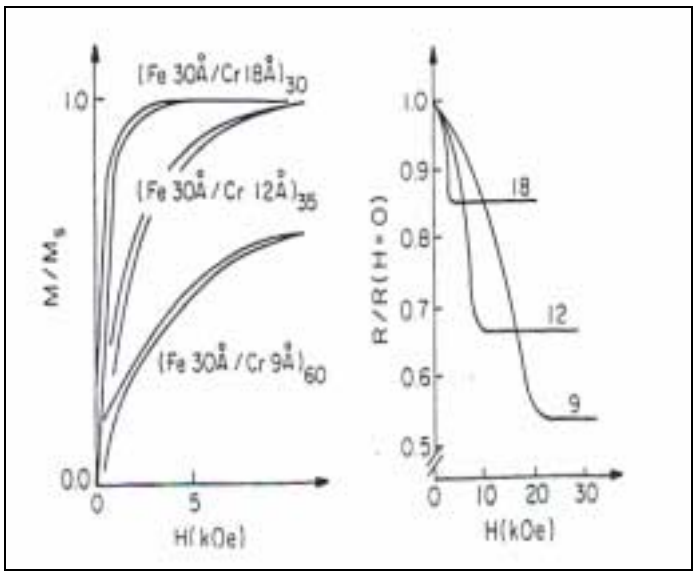

Figure 2.1: Left graph gives hysteresis loop from different Fe/Cr structures. Right graph gives the relative change in resistance for different thickness of Cr spacers [Baibich *et al*. (1988) [2]].

2.2 Definition

As it was noted above, GMR is the abrupt change in resistance in magnetic multilayer structures when an external magnetic filed is applied. There are two ways of measuring the change in resistance. Both methods describe the GMR change but one has the saturation magnetic field as reference point where the other has the zero point of the magnetic field. The first convention applies to antiferromagnetic configuration and is never more than 100% whereas the second convention refers to ferromagnetic configuration, which is used in calculations [3].

The following equation gives the change in resistance calculated with the second convention:

$$\frac{\Delta R}{R} = \frac{R_{AF} - R_F}{R_F} \qquad (2.1).$$

The importance here is that for large changes in resistance, the two methods deviate from each other in greater amounts. The structures themselves consist of magnetic and non-magnetic layers. The magnetic layers are made from ferromagnetic materials (Cobalt, Iron, Nickel, and alloys of the above). The non-magnetic layers are usually made from Chromium, Copper, or Silver. The non-magnetic layers are known with another identity, namely spacers. The thickness of these spacers is very crucial to the GMR effect, as it would be shown in the next few pages.

The GMR effect is greatest when an antiferromagnetic arrangement of magnetizations in the multilayers changes into a ferromagnetic one. This happens because GMR depends on the relative orientation of the magnetizations of the successive magnetic layers and therefore in the electron-structure match between these layers [12]. In the next few pages, the mechanism of GMR is explained and the above statement becomes more evident.

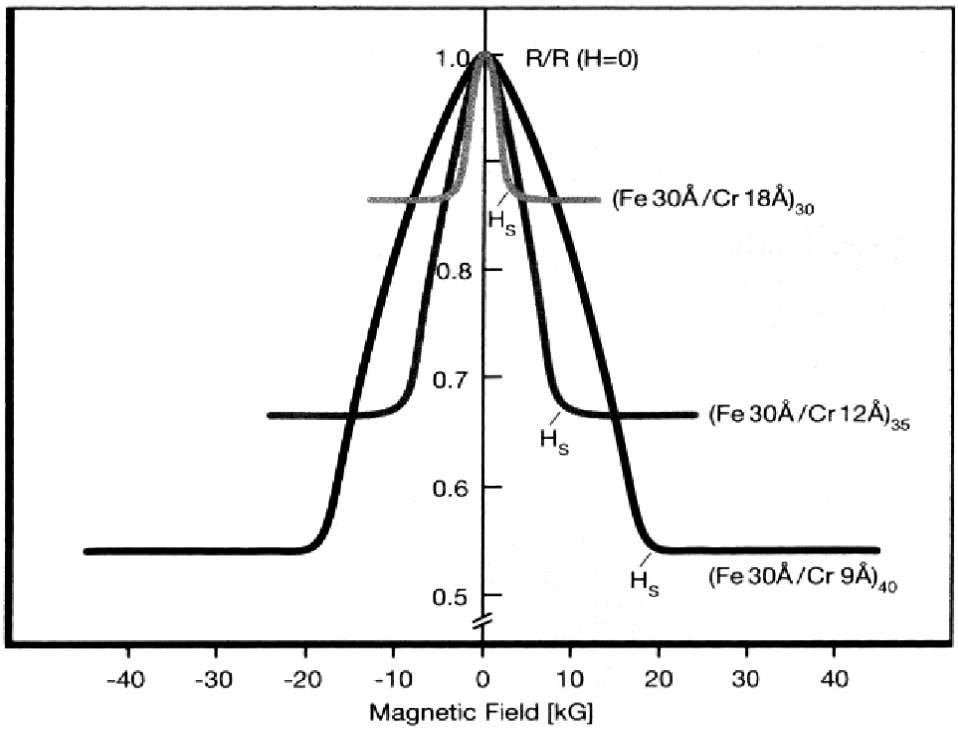

Figure 2.2: Resistance change versus external field for different repetitive multilayer structure. Note that more repetitions yields greater GMR effect. [4]

The GMR effect is greatly enhanced in a repetitive multilayer structure, which suggests that the interfaces of the layers are important. Figure 2.2 shows the effect of a repetitive multilayer structure on the GMR effect. To this day, there is a debate about the role of the interfaces. The issue in question here is that there is an uncertainty about the origin of the electron scattering. Different leading scientists believe that either the scattering comes from the interface or from within the bulk of the layers or even that both cases are true. In 1992, Parkin *et al* constructed multilayers of Permaloy and Copper ($Ni_{81}Fe_{19}$/Cu) and coated their

interfaces with Cobalt (Co) and then studied their properties [5]. Different thicknesses ranging from 0 to 4.4 Å were used and as a result, the GMR increased from 1% to 20% at room temperature [2]. They particularly found that when the Co thickness reached 4 Å, the inside combination layer NiFe/Co is of no importance. In fact, the multilayer {Co/Ni/Fe/Co/Cu} acted as Co/Cu at room temperature [2]. The importance of multilayer's interfaces seems to be more important than the bulk of the layers themselves as far as the electron scattering is concerned.

2.3 Moke Graphs

Magneto-optic kerr effect (MOKE) graphs give the change in magnetization as a function of the applied external field. This change of magnetization is measured as a small rotation of the polarization of light traveling through a magnetic material. Changes is the linear susceptibility of the materials with applied magnetic field underlie the fundamental principles of the linear MOKE phenomenon. This effect is used extensively in research studies and magnetic thin film applications [4]. Without going into detailed analysis of this subject, it should be noted here that the MOKE signal is in a good approximation and proportional to the ferromagnetic magnetization, which serves as an experimental verification of the GMR effect. Such a MOKE signal (bottom part) and the respective change in resistance graph (top part) are shown if figure 2.3.

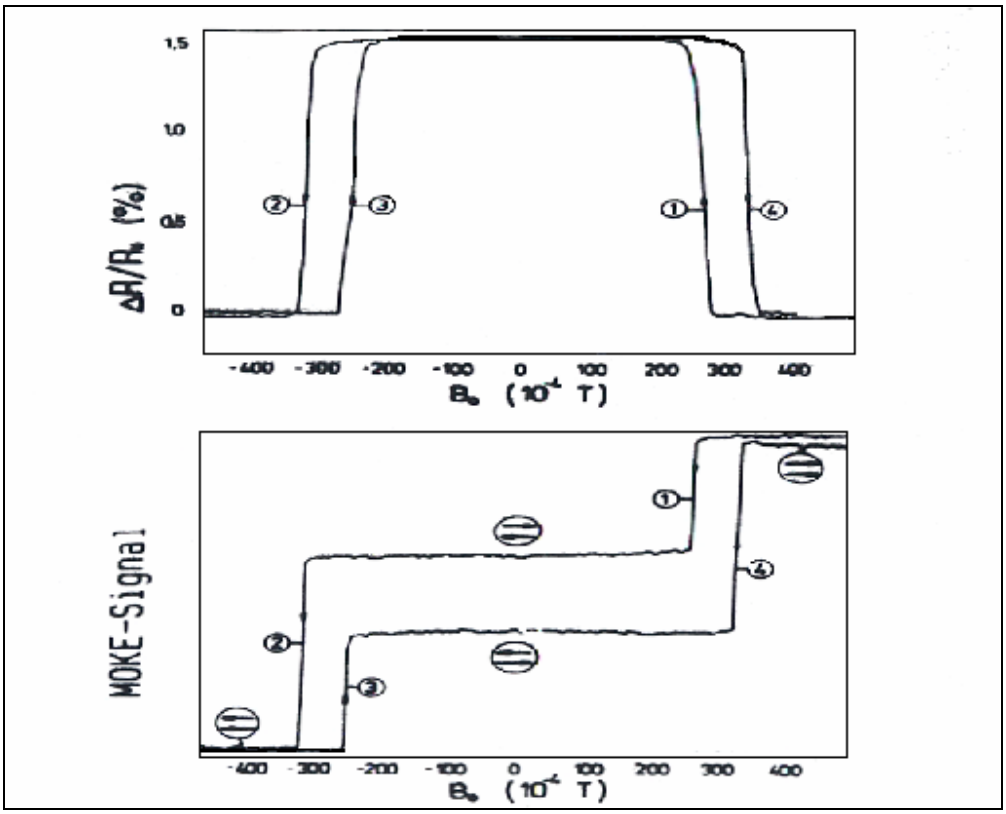

Figure 2.3: MOKE graph hysteresis loop (bottom) and its respective change in resistance graph (top) from {Fe(120Å)/Cr(140Å)/Fe(120Å)} multilayer with antiferromagnetic coupling. [P. Grünberg *et al.* (1990)].

2.4 Angle Between Magnetizations

The GMR depends on the angle or relative orientation between adjacent magnetic layers as opposed to anisotropic magnetoresistance (AMR) that depends on the relative position of magnetizations and current. Consequently, GMR is essentially a measure of the angle between magnetizations. Specifically for small angles, the change in resistance is low and for large angles (up to 180°) the change in resistance becomes also large. This effect is illustrated in figure 2.4. This angle

dependence is the driving force behind the oscillatory coupling between magnetic layers that in turn gives rise to the GMR effect. This coupling oscillates between ferromagnetic and antiferromagnetic layers depending upon the angle between successive ferromagnetic layers.

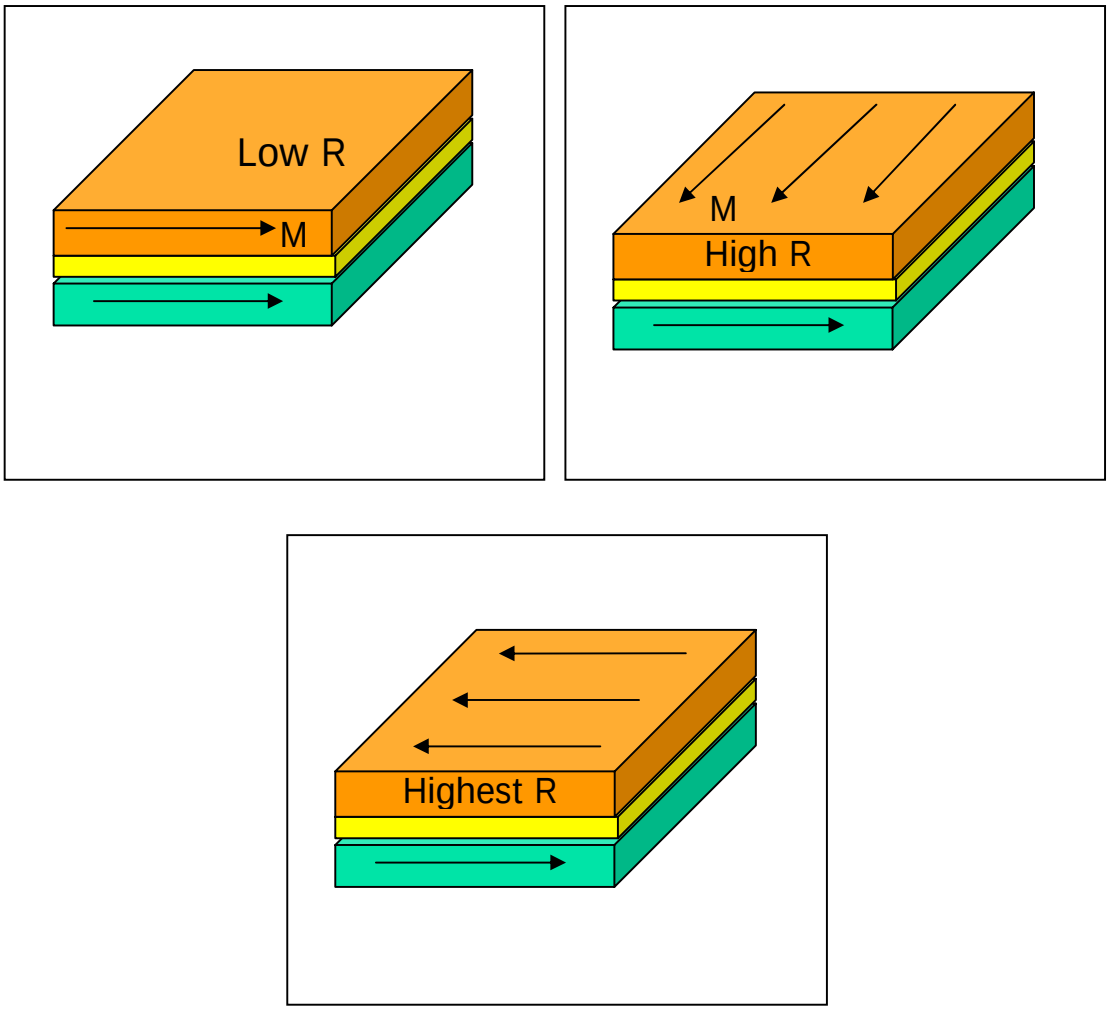

Figure 2.4: The angle between the magnetizations reflects the change in magnetoresistance. Low resistance corresponds to ferromagnetic coupling (upper left), high resistance into anything between angle (upper right), and antiferromagnetic one case with the highest change of resistance (lower center).

The equation that relates the change in the resistance and the angle between magnetizations of two successive layers was developed by Dieny *et al.* [17, 18]. It has the following form:

$$\frac{\Delta\rho(\psi)}{\rho} = \left(\frac{\Delta\rho}{\rho}\right)_{GMR} \frac{1-\cos\psi}{2} \qquad (2.2).$$

Here ψ is the angle between ferromagnetic-layered materials, ρ is the resistance at the reference magnetic field, and $\Delta\rho$ the change of resistance.

2.5 Spacer Dependence of GMR

In order to get an antiferromagnetic configuration of the magnetic layers, a spacer must be present between adjacent magnetic layers (for a ferromagnetic configuration one only needs to apply strong enough current to align parallel the magnetizations). The coupling between the successive magnetic layers oscillates as a function of spacer thickness. The importance here is that the spacer needs to be a certain thickness (few Å) in order to get an antiferromagnetic configuration. This is clearly seen in figure 2.5. Parkin *et al.* (1990) [5] observed this oscillatory graph of magnetoresistance as a function of spacer (Cr) thickness in Fe/Cr multilayers. The magnitude of magnetoresistance ratio and the magnitude of the field needed to saturate the magnetization are found to be in phase [3].

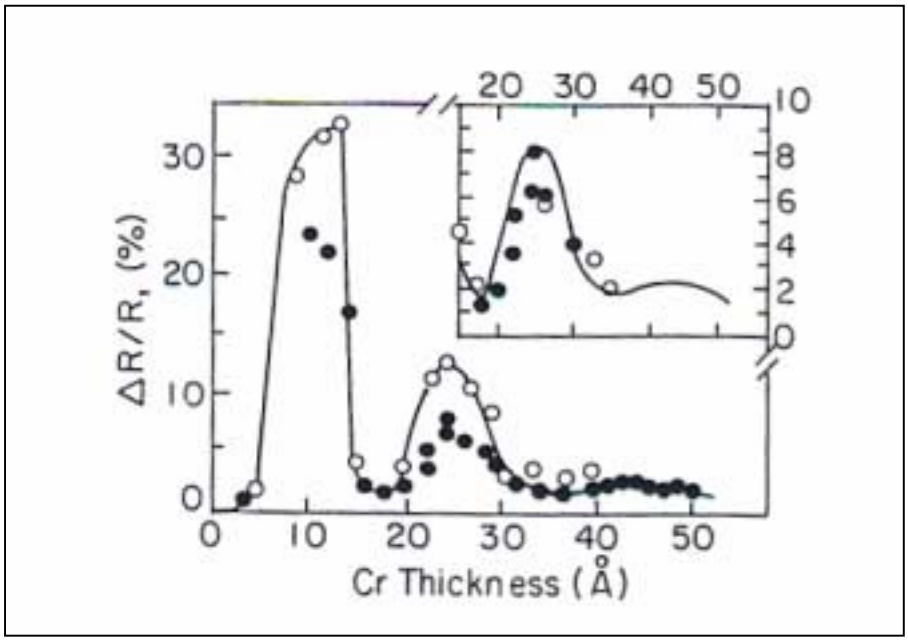

Figure 2.5: Change in MR as a function of the spacer thickness from Fe/Cr multilayers at 40°C and N=30 repetitions (closed square) and 125°C and N=20 repetitions (open square) [Parkin *et al.* (1990) [5]].

2.6 Experimental Verification of Spacer Dependence

An experimental verification of GMR's spacer-dependence is established in the following graph, which was kindly obtained from Stoner labs at Leeds, UK. The dependence of GMR on Cu spacers is demonstrated in figure 2.6. The three peaks visible in the graph illustrate this idea. For large thicknesses, the GMR is small because the magnetic layers are not coupled. As the thickness of Cu gets smaller, the effect becomes increased for certain values of these thicknesses. For Cu thickness of 9 Å, which is about three Cu atoms thick, the effect is largest.

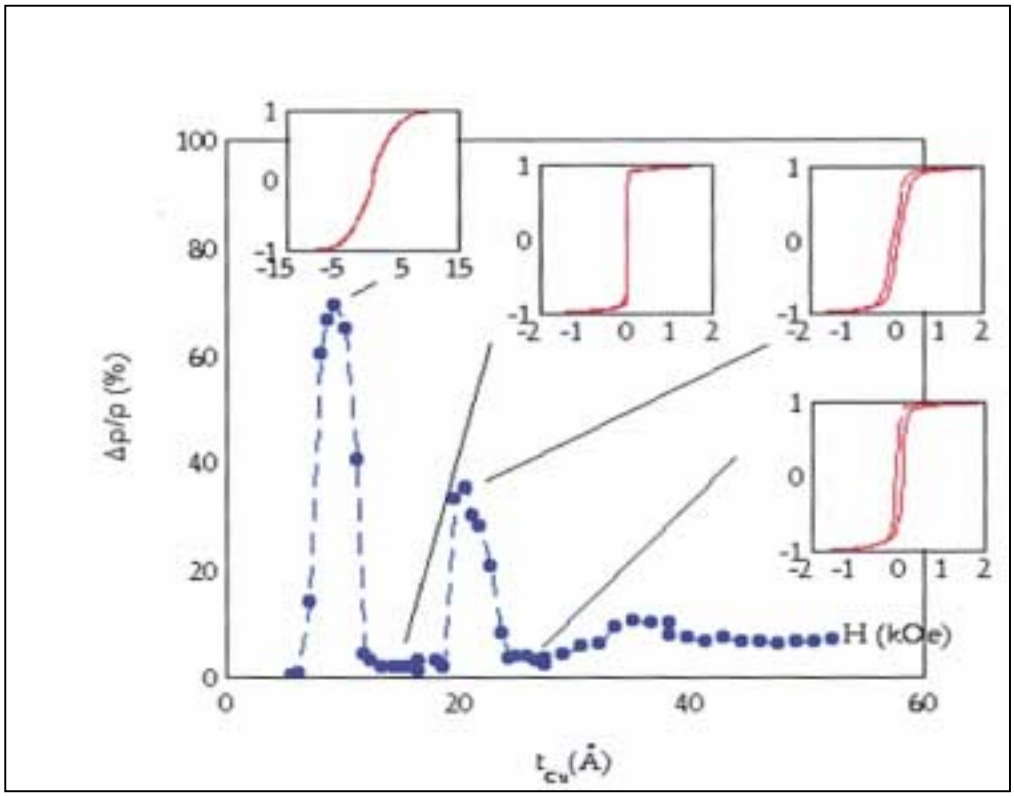

Figure 2.6: The spacer dependence of GMR effect. The MR maximum occurs at Cu thicknesses where the magnetic layers at antiferromagnetically coupled. The inserts show the various hysteresis graphs for each Cu thickness. [www.stoner.leeds.ac.uk (2003)].

2.7 Mechanism of GMR

Analogically, the GMR effect is similar to the one of polarization of light. In this effect, light is allowed to pass thru two polarizing lenses when the polarizers align parallel to each other and block light when the do not align with each other. Similarly, when the magnetizations of two magnetic layers tend to align, the resistance drops to very low levels and the vise versa is true. For ferromagnetic configuration (see figure 2.7 next page), one of the spin carriers

(electrons) passes thru both the magnetic layers with no scattering (resistance), but the other spin carrier scatters at both layers since there is a mismatch of the electronic structure of its spin and the magnetization of the layers. In an antiferromagnetic configuration, both electrons encounter scattering. The spin up electron as depicted in figure 2.8 scatters at the second layer and the spin down at the first layer.

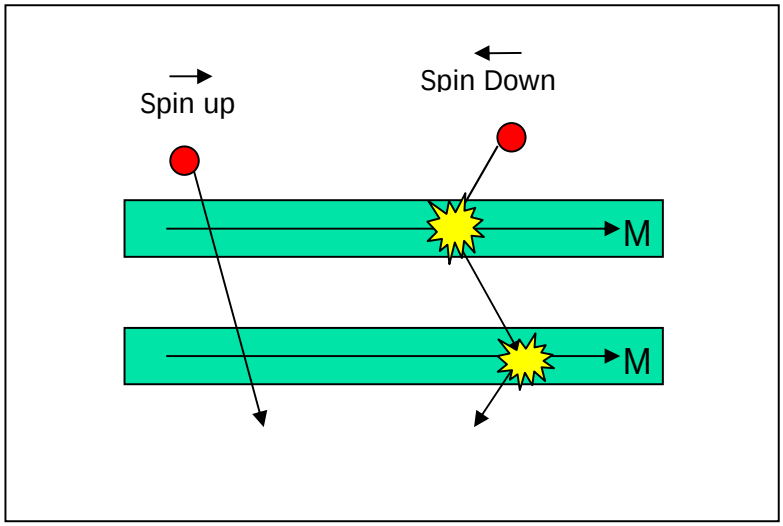

Figure 2.7: Ferromagnetic configuration that results in low resistance.

The overall effect is that the resistance in the antiferromagnetic case is larger than the ferromagnetic configuration. It should be noted here that figures 2.7 and 2.8 depict current perpendicular to the plane (CPP) as oppose to current into the plane (CIP). The CPP mode indicates that the current is flowing perpendicular to the magnetization of the ferromagnetic material. The CIP mode,

as the name suggests, indicates current parallel to the magnetization of the magnetic layer. Theoretical models predict GMR values much higher for CPP than the CIP mode [19]. Electrons in this mode must transverse multiple magnetic layers resulting in a higher magnetoresistance. However, constructing GMR sensors using CPP mode is a tough challenge that has not seen practical realization. However, a combination of these modes yields a new mode called current into angle to the plane (CAP). This mode is the essential part of this project meaning that our embossed surfaces yield the desired CAP mode for GMR effect. Corrugated and V-grooved substrates have been used [7, 20, 21, 22, 23] to investigate CAP mode. The results show a value of GMR higher that the CIP mode but lower than the CPP mode. Levy has done some theoretical calculations [24] in order to explain the enhancement of the GMR effect thru new substrates.

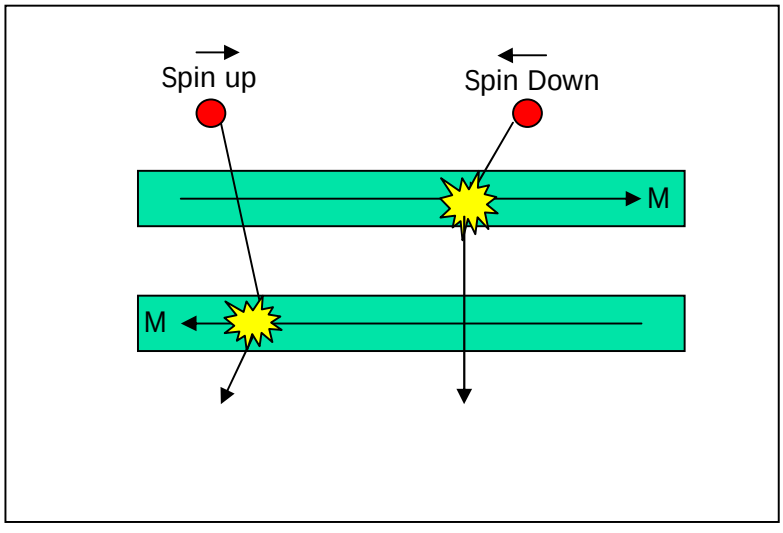

Figure 2.8: Antiferromagnetic configuration that results in high resistance.

2.8 Mott's Two Current Model

The arrangements depicted in figures 2.7 and 2.8 can be visualized in a circuit arrangement that is based on the Mott's two current model. The ferromagnetic configuration of figure 2.7 will look as in figure 2.9 following a simple circuitry approach. In this case, the Mott's two current is calculated from this equation:

$$R_F = \frac{2 R_1 R_2}{R_1 + R_2} \quad (2.3).$$

Here, R_1 is less than R_2 because the spin up electron encounters no scattering from the magnetic layers. In the antiferromagnetic case, the high resistance is given by the following equation:

$$R_{AF} = \frac{R_1 + R_2}{2} \quad (2.4).$$

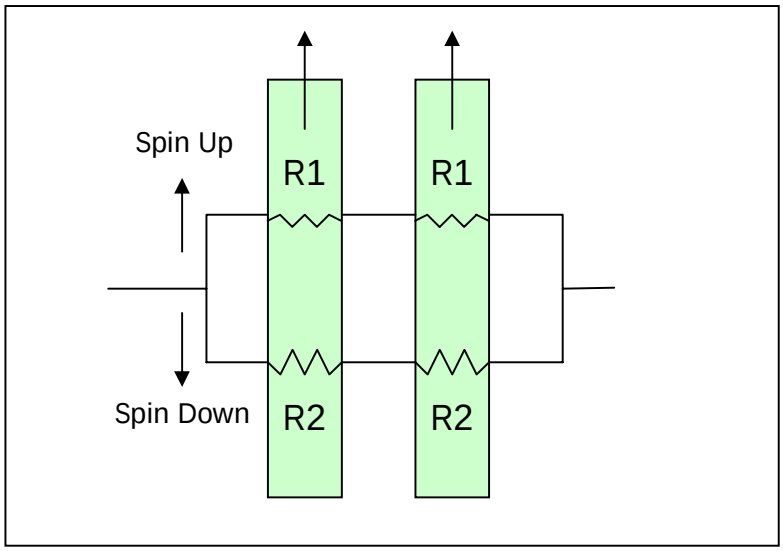

Figure 2.9: Ferromagnetic configuration equivalent circuit.

In any case, equation (2.4) is always more than (2.3) and this is what makes the magnetic multilayered structures achieve the GMR phenomenon. With equation (2.1):

$$\frac{\Delta R}{R} = \frac{R_{AF} - R_F}{R_F} = \frac{(1-\alpha)^2}{4\alpha} \quad (2.5).$$

Here α is the asymmetry scattering parameter defined as:

$$\alpha = \frac{R_1}{R_2} \qquad (2.6).$$

An antiferromagnetic circuit representation is depicted in figure 2.10.

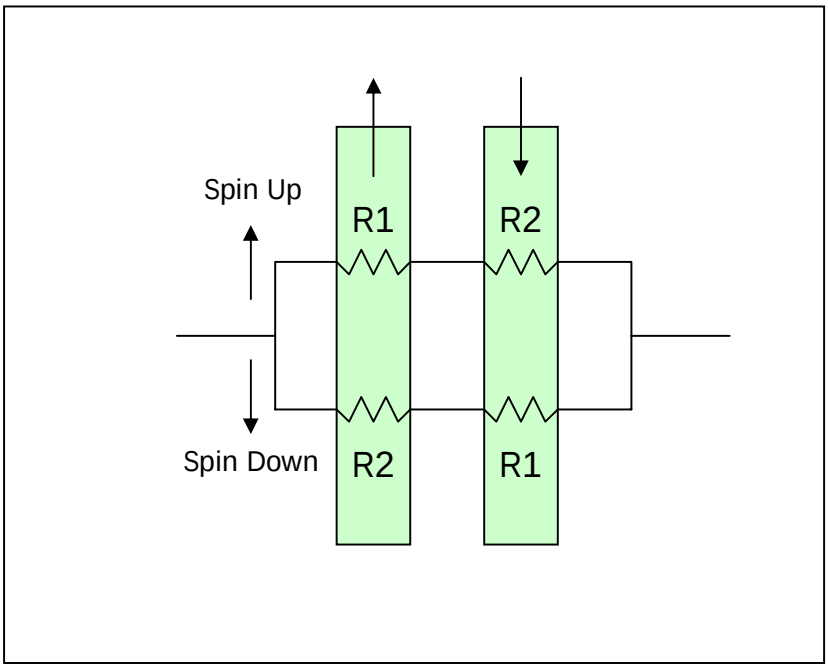

Figure 2.10: Antiferromagnetic configuration equivalent circuit.

It should be noted that when R_F is less than $R_{AF,}$ the MR ratio is positive. The MR ratio can be positive or negative depending on different ferromagnetic layers. Furthermore, for maximum GMR, the thickness of the ferromagnetic and antiferromagnetic layers should not be more than a few tens of Å, i.e. less than the mean free path for inelastic scattering of the conduction band electrons [6].

2.9 Multilayer Repetition

As it was noted previously, the GMR effect is greatly enhanced if the magnetic and non-magnetic multilayered is repeated many times (as many as 100 times depending the particular structure). An antiferromagnetic multilayer repetition structure greatly enhances the increase in resistance because the electrons will scatter many more times compared to a single multilayered structure. A repetitive antiferromagnetic multilayer configuration is shown in figure 2.11. These scattering events are taking place much more often and the net result is a greater GMR effect. It should be noted that the scattering events are not due to electron-electron interactions that takes place at the end of the mean free path of the electrons, which is defined, as the average distance an electron will travel between scattering events. The GMR effect rather comes from interaction of the electron spin and scattering site spin [3]. In the ferromagnetic case, the opposite happens. Electrons will scatter much less thru the magnetic layers and

the GMR effect is diminished since the resistance disappears. In actuality though, the resistance does not completely disappear but rather the change in resistance drops to very low levels. A repetitive ferromagnetic multilayer configuration is shown in figure 2.12.

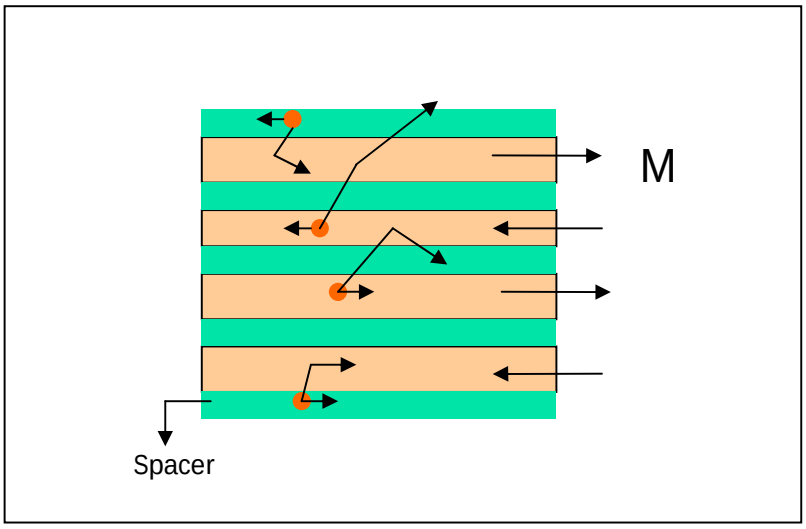

Figure 2.11: *An* antiferromagnetic multilayer repetitive configuration.

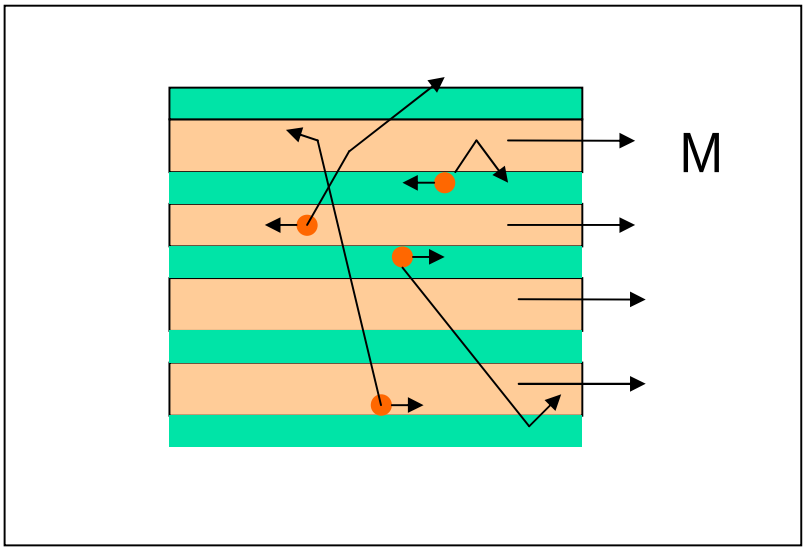

Figure 2.12: *A* ferromagnetic multilayer repetitive configuration.

2.10 Spin Polarization in Layers

As mentioned in the last paragraph, the ferromagnetic configuration allows electrons to travel freely thru the layers. This has to do with the spin polarization in the spacers. The electronic polarization is the same as the electronic spin, namely the spin-spin interaction of the electron and the scattering site. Spins in ferromagnetic material can easily flow and saturation of the magnetization is easily obtained as shown in next page in figure 2.13. On the other hand, an antiferromagnetic multilayer does not allow for an easy flow of the electrons thru the layers. This is because the energy needed to overcome the scattering potential is greater than the one from a ferromagnetic configuration. This is depicted in figure 2.14 in the next page. Note that the electrons do flow from the first layer to the spacer, but they scatter on the interface between the second layer and the same spacer due to different spin polarizations.

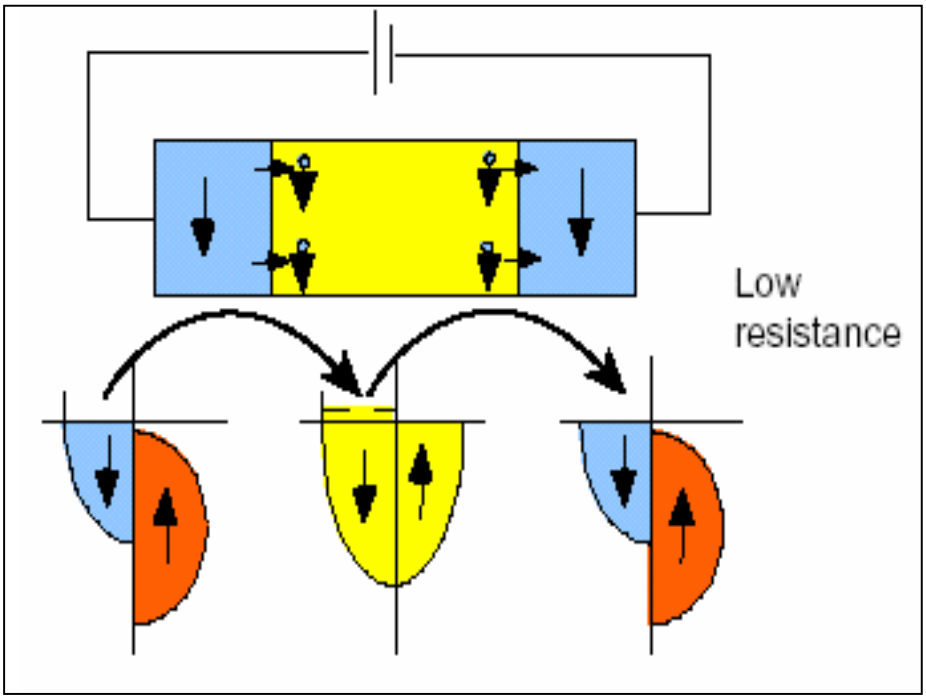

Figure 2.13: *A* ferromagnetic multilayer allows for easy electron flow.
[Prinz, Science **282,** 1660 (1998)].

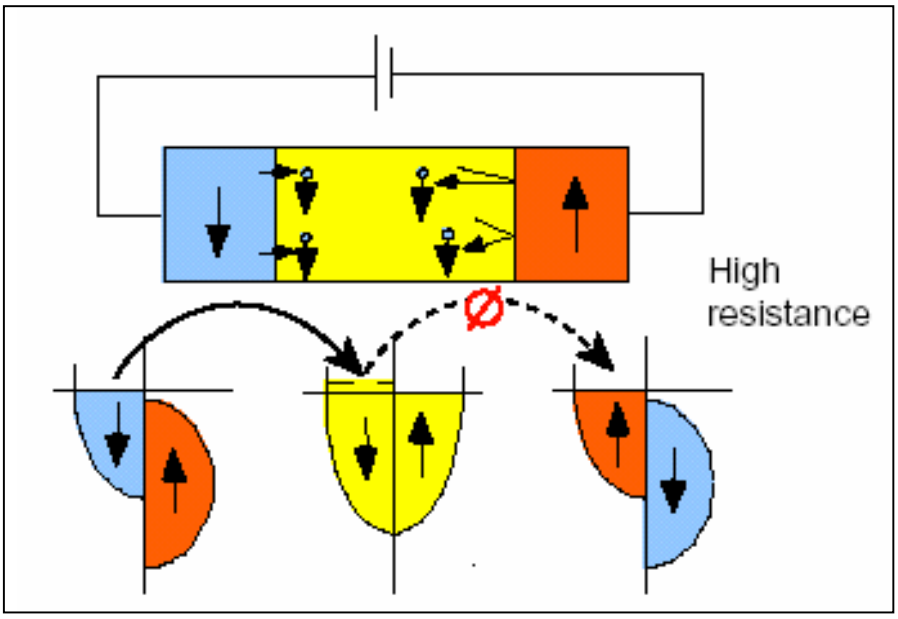

Figure 2.14: An antiferromagnetic multilayer does not allow for easy electron flow.
[Prinz, Science **282,** 1660 (1998)].

2.11 Applications

GMR has been the subject of numerous technological achievements. The applications range form GMR sensors (also known as Spin Valves), Spin Switches, detection of landmines, non-volatile electronics such as MRAM, and many more. Read GMR Heads for data retrieval are increasingly sensitive which yield higher data densities for hard drives. The principle behind them is the mechanism of GMR, which allows for higher sensitivity due to the change of resistance. The basic structure of a GMR hard disk head sensor is shown in figure 2.15. Note that the mode is CIP since a CPP is not practically feasible.

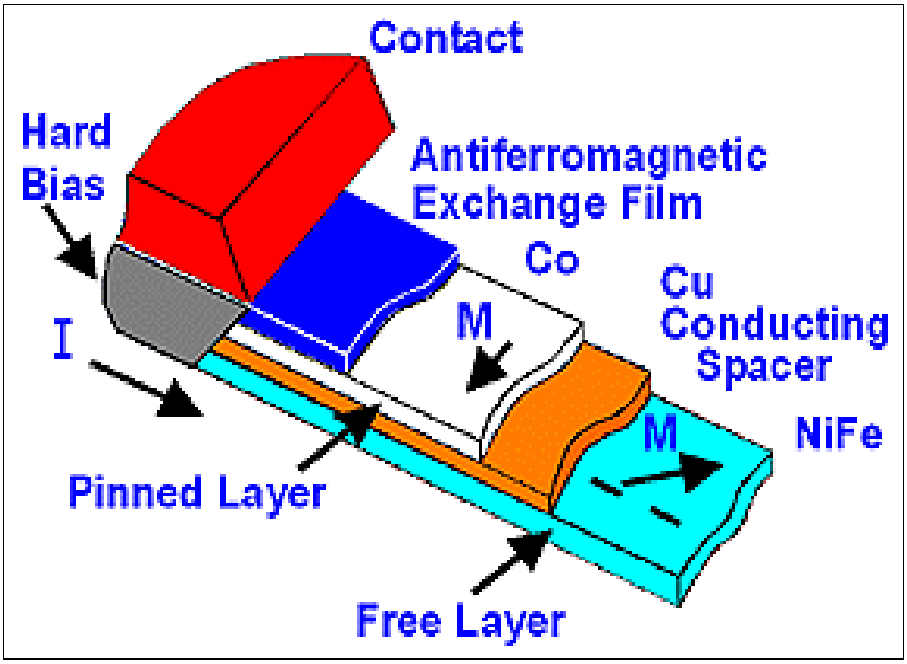

Figure 2.15: Principles of GMR read head sensor. [Kindly provided by Hongmei Luo in Chemical Engineering, Tulane University]

When the zero read bit passes underneath the GMR sensor, nothing happens because the magnetic flied is not in the direction of the magnetizations of the magnetic layers. However, when the read bit 1 passes underneath the GMR head, the external magnetic field changes the magnetization of the free layer and this results in drop of resistance and hence an increase in current. This makes the GMR head sensor very responsive. Due to his effect, today virtually all hard drives are made with GMR read sensors. This in turn gives the opportunity to manufacture hard drives of greater densities, which is a must in the current market of hungry-for-storage consumer market. This point is illustrated in figure 2.16.

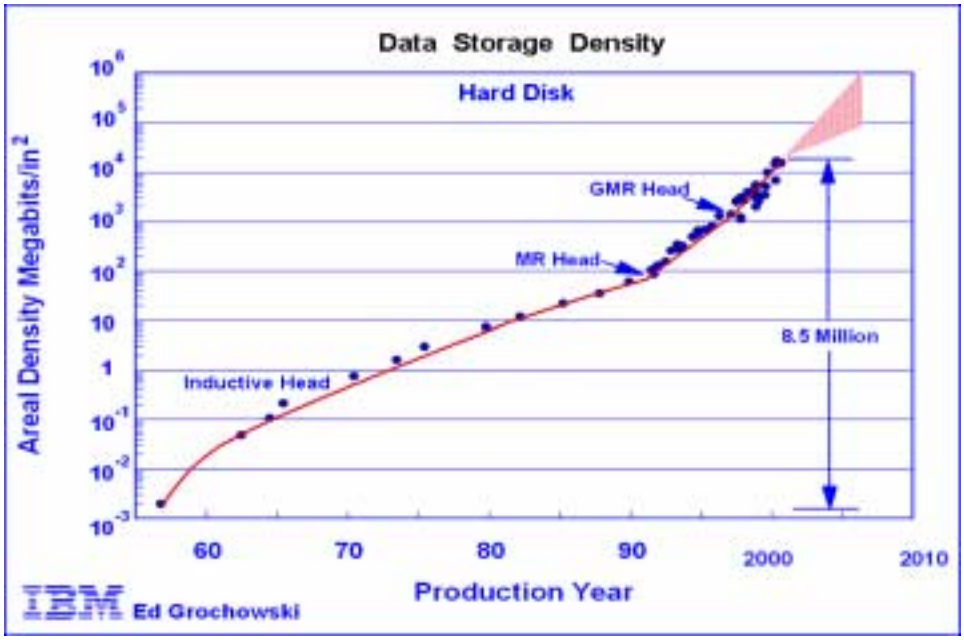

Figure 2.16: Areal Density comparison for different read heads.
[Source: IBM®].

Another very important application of the GMR effect is in non-volatile electronics. MRAM is a premium example of this. While still in the development stage, it is deemed the next revolution in memory applications. There are different designs for MRAMs. The one discussed here is composed of two layers: the upper-a soft magnetic layer, and then lower-a hard magnetic layer. These MRAMs were pioneered from Schwee, Phm (1991), and Daughton (1992) [references within 3]. In the write process, the information is stored in the lower layer by applying a strong magnetic field. In the read process, a low intensity magnetic field is applied to change the magnetization of the top layer thus reading the information stored in the memory. This example is illustrated in figure 2.17.

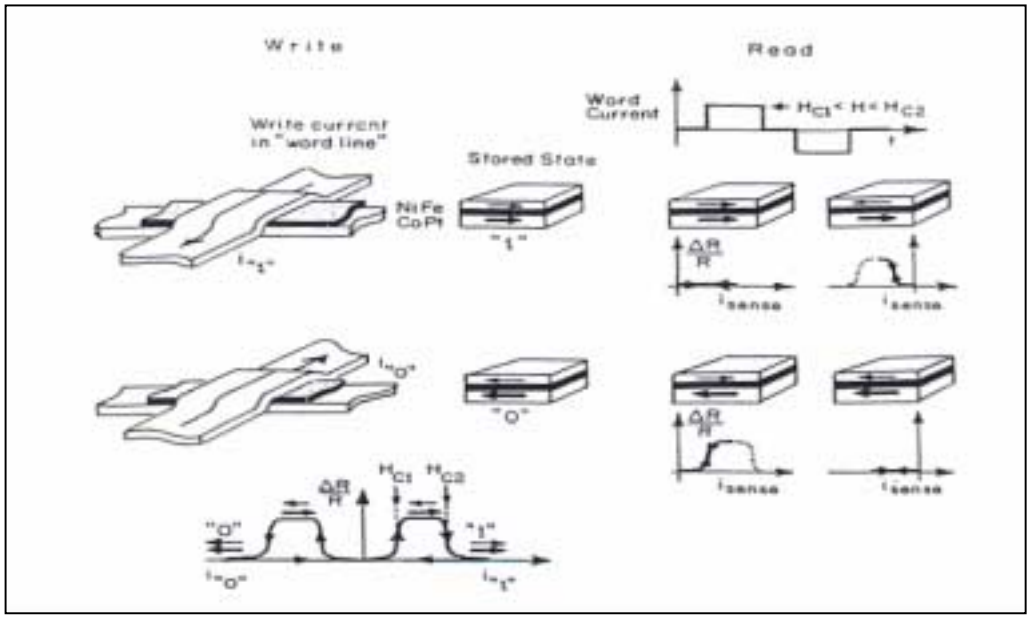

Figure 2.17: Diagrams of the write and read functions of MRAM [3].

Perhaps, the most important future of the MRAM is its non-volatile function. When power is lost or turned off, the memory does not loose its magnetization and thus the information that might be stored. Of-course this is a welcoming advantage since current random access memories do loose their information if power is lost.

CHAPTER 3

Initial Experimental Setup

3.1 Substrate Preparation

The substrates used for the structures that where studied for the improvement of the GMR effect in this thesis were fabricated from high purity (99.999%) aluminum (Al) that. Al sheets were initially treated with acetone in order to eliminate any surface contaminations that might have been present. The sheets were immersed in the acetone bath for twenty minutes and degreased by the method of ultrasonication. Subsequently, the Al sheets were annealed in argon (Ar) at 350 °C for five hours where the internal stresses were removed, and the Al became stronger through the gradual increase and decrease of the temperature. The use of argon also promoted the smoothness and flatness of the Al surface. The natural occurring aluminum oxide monolayer on the surface of the Al sheets was removed before anodization. Then, the Al sheets were electropolished in a 1:4 volume mixture of perchloric acid ($HClO_4$) and C_2H_5OH, respectively. The electrodeposited Al sheets were next anodized for twelve hours at 17 °C in a 0.3 M oxalic acid with an applied voltage of 40 volts. Consequently, the porous membrane (AAO) of Al_2O_3 was formed with diameter of 60 nanometers (nm) and 100 nm regular spacing. The thickness of the membrane was ultimately controlled

by the current density and anodization time. However, the quality of very thin membranes was very unsatisfactory for the high demands of the project. Therefore, a new technique had to be used in order to produce high quality membranes. Thicker membranes were first manufactured following the above procedure and subsequently the oxide membranes introduced on the Al sheets were removed by immersing the whole structures in an aqueous mixture of phosphoric acid (5 % wt) and chromic acid (1.8% wt) at a temperature of 70 °C. The structures remained in the mixture for fifteen hours. An illustration of the processes involved in the manufacturing of the substrates is shown in figure 3.1.

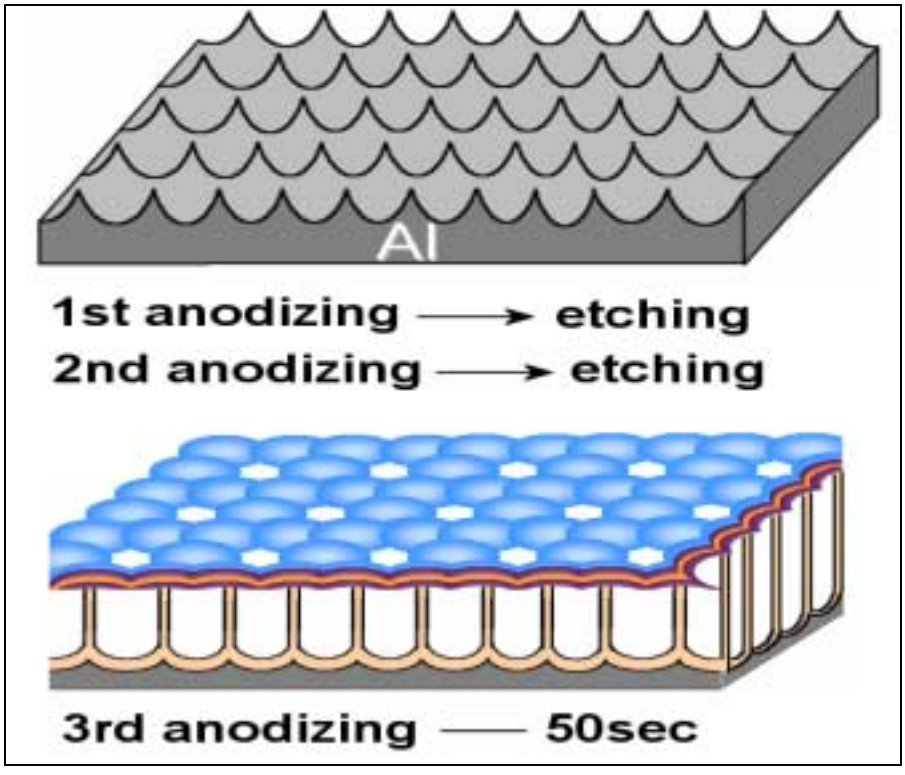

***Figure 3.1*:** Schematic representation of the preparation of the embossed alumina surface (top) and an isometric diagram of the AAO profile (bottom).

The above procedure of anodization and etching depicted in figure 3.1 was repeated twice. A final anodization was applied for only 50 seconds, which yielded the desired depth of the membranes. This depth was in the same order of magnitude as the pore spacing. Actual measurements produced a pore depth of about 280 nm. These embossed surfaces were the substrates used in the sputtering deposition (chapter 4) producing the new enhanced GMR sensors.

3.2 Surface Topology

The different geometry of these surfaces from other flat surfaces or even V-grooved surfaces used in previous GMR sensors almost certainly guaranteed a promising research in front of our group. The suitability and pioneering surface for GMR sensing was on the best ways to start improving a phenomenon widely used in the technology sector. Reproducibility and continuity of the surface with no defects was crucial since surface "noise" could diminish the effect. The nice hexagonal surface arrangement is shown in figure 3.2. Perhaps the regular hexagonal arrangement is more evident in figure 3.3 where the depth is also clearly visible. These atomic scale pictures verified our expectations that the surfaces have regular hexagonal geometry and continuity. This geometry is shown in figure 3.4.

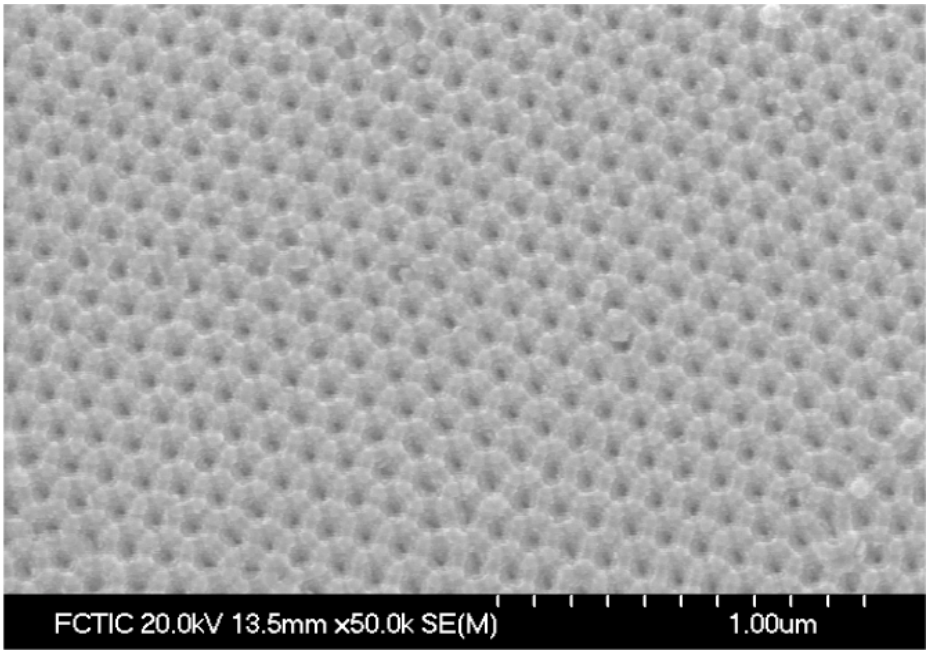

***Figure 3.2*:** Top view of the embossed surface using Scanning Electron Microscopy (SEM).

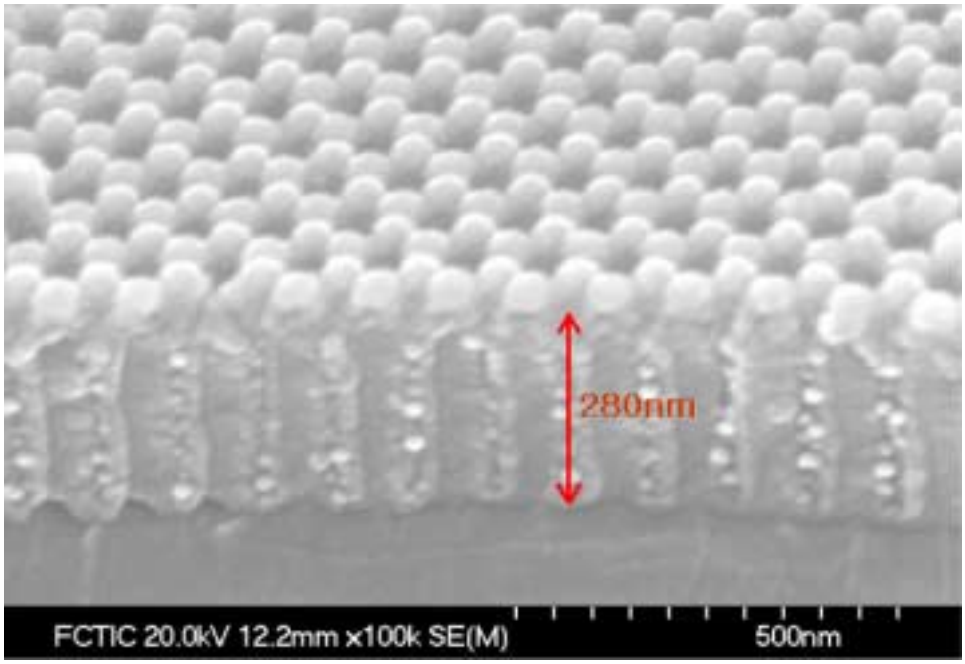

***Figure 3.3*:** Large zoom isometric view of the embossed surface using (SEM).

Even though it can be visible small defects are present on the surface, they should not be a major factor in the overall performance of the GMR structures. At this scale man-made structures are deemed to be imperfect due to technological limitations. However, in the near future we might be able to fabricate structures with no defects and of any shape. Nevertheless, the fabricated surfaces were deemed to exceed our requirements, and we proceeded with a final step before the actual deposition of the magnetic and non-magnetic materials on the surfaces. That step was to verify the geometry of the surface using a more powerful topographical instrument than the scanning electron microscope (SEM).

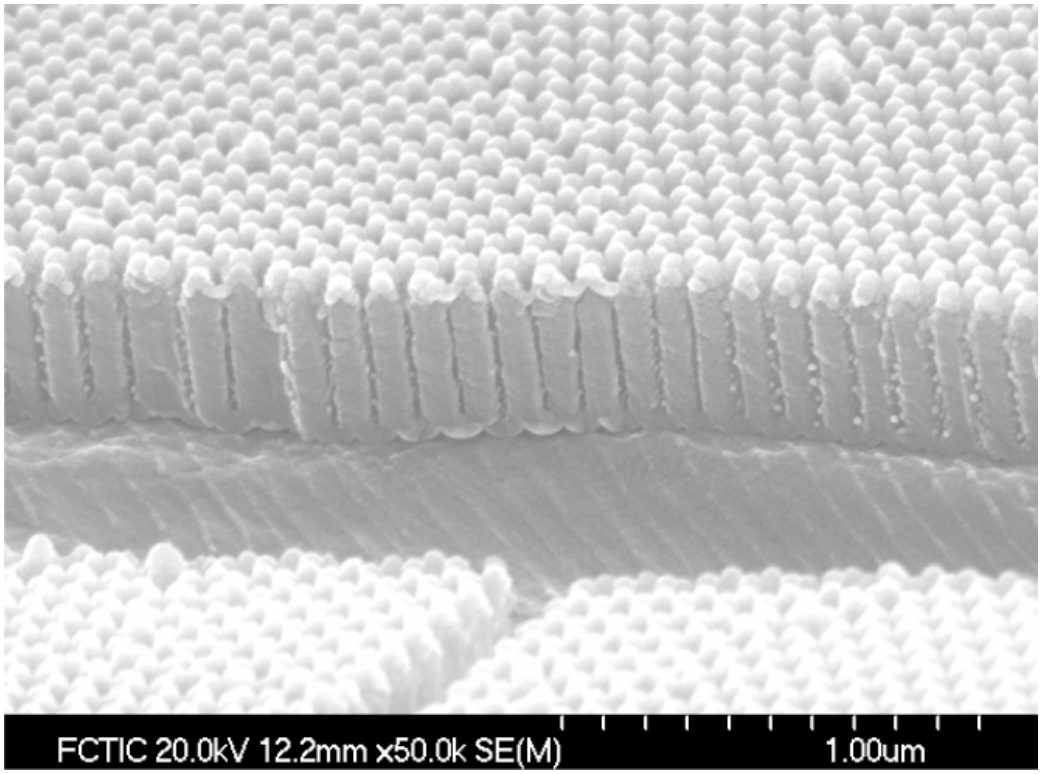

***Figure 3.4*:** Zoomed-out isometric view of the embossed surface using SEM. Note the small imperfections, which are thought not to contribute in any major way to the GMR effect.

Atomic force microscopy (AFM) was used (with many thanks to professor Carl Ventrice for his assistance with the operation of the AFM) to verify the topography of the surface. The AFM model used is Nanoscope IIIa, built by Digital Instruments, and belongs to AMRI, UNO. The amazing detail obtained by using this apparatus enabled us to be completely convinced that the substrate was the desire one. Careful studies and numerous samplings form different areas on the embossed surfaces showed the regular hexagonal arrangement anticipated. Several snapshots of the AFM photographic mode were taken and analyzed within the program of the apparatus. Vertical scale, pore diameter, and overall continuity of the surface were examined. All the results were conclusive and pointing towards the validity of the AAO embossed surfaces. In figures 3.5, 3.6 and 3.7, the surfaces are shown in different length scales and different AFM viewing modes to emphasize the pores.

After all topographical measurements were done, we moved to the next and most important step of this project: the actual deposition. However, we accentuated the surface geometry to the extend that we were certain that we had the desired surface since a different surface geometry could jeopardize the success of the whole project.

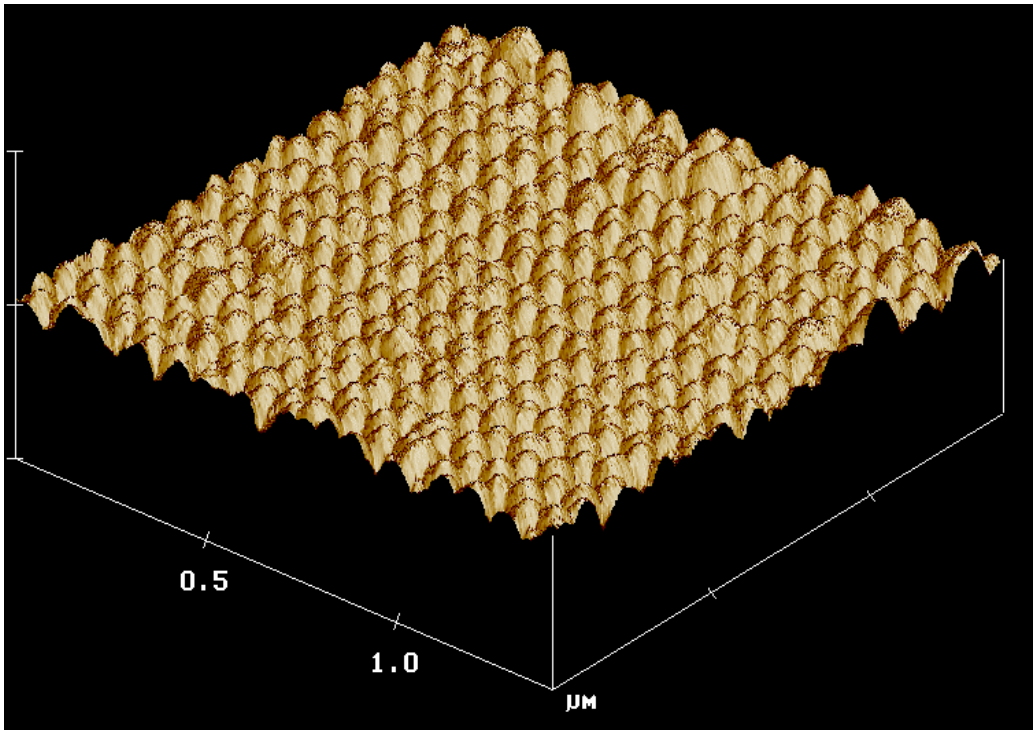

***Figure 3.5*:** Zoomed-out isometric view of the embossed surface using AFM.

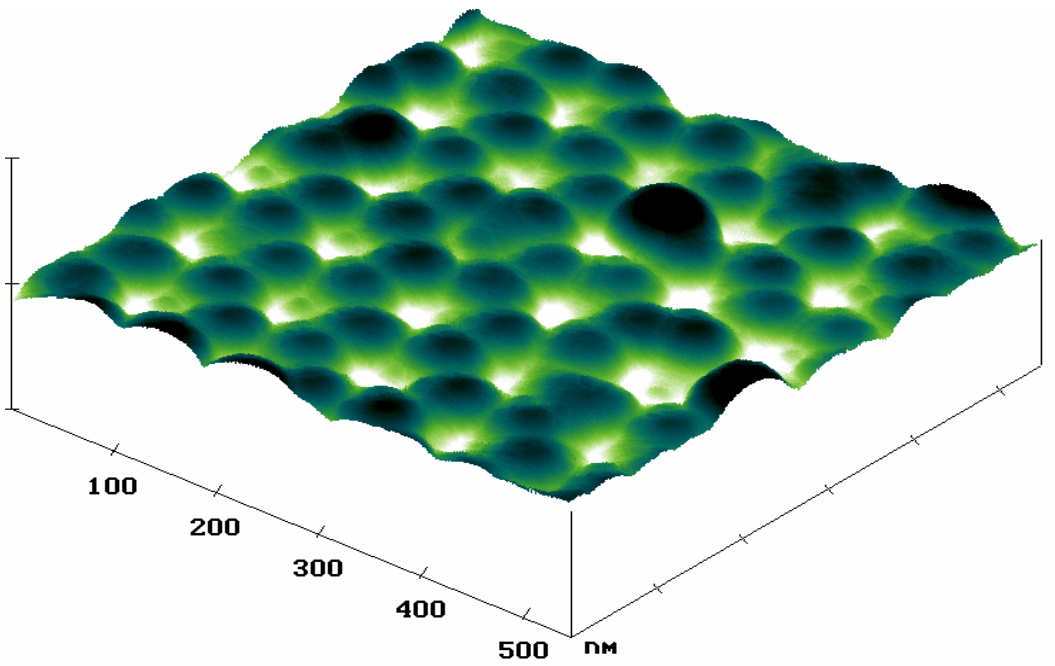

***Figure 3.6*:** Zoomed-in isometric view of the embossed surface using AFM. Note the amazing detail and clear presence of the pores. The length scale is also evident.

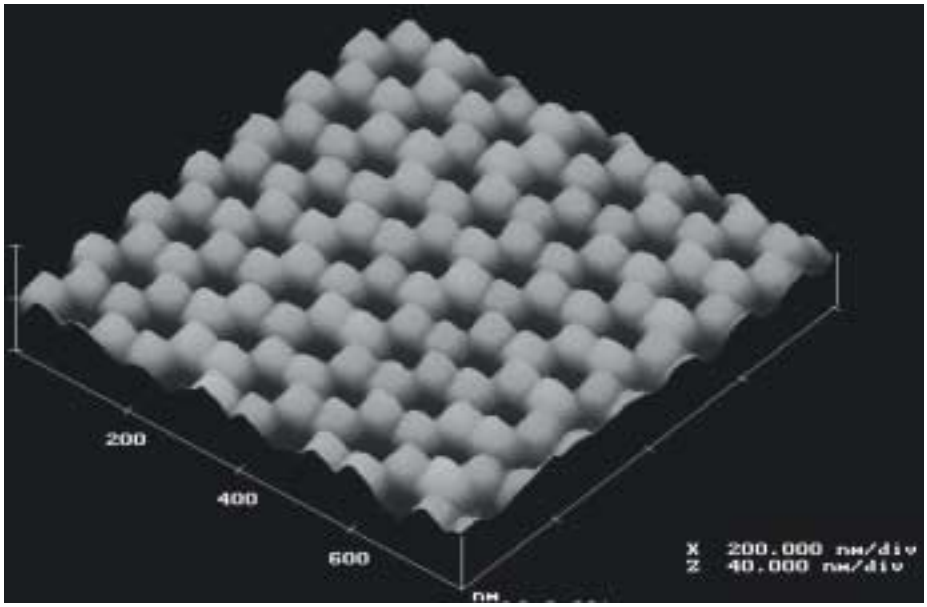

***Figure 3.7*:** Isometric view of the embossed surface using AFM. The goal here was to emphasize the regular hexagonal pattern.

CHAPTER 4

Deposition Process

4.1 Choice of Deposition System

After it was clear that the substrate surface was the desired regular hexagonal array with pore diameter of about 60 nm and spacing of about 100 nm, we proceeded with the actual deposition of the magnetic and the non-magnetic multilayers. The deposition of the films was done using DC-magnetron sputter supplied with S-research target guns. The Thin-Films laboratory, under the management of the Advanced Materials Research Institute (AMRI) and supervision of professor Leszek Malkinski, was the placement for carrying out the deposition experiments. Located at the second floor of the Science building at the University of New Orleans (UNO), the lab was fully equipped to carry out such experiments. The advantages of the DC-magnetron sputter were a decisive factor in choosing the deposition technique. Such advantages include the uniformity of film thickness [8, 9], which was one of the most important considerations bearing in mind that the spacer thickness (in this case copper (Cu)) is the reason for antiferromagnetic or ferromagnetic coupling. In other words, the GMR effect directly depends on the Cu thickness and that thickness had to be uniform throughout the deposited surfaces. The ability for good

adhesion to most surfaces with DC-magnetron sputter was another key parameter in choosing the deposition method. The films of either cobalt (Co) or copper (Cu) had to adhere to each other and more over the films had to adhere to the substrate of aluminum oxide (AAO). Especially iron (Fe), which was used as the seed layer for further adhesion improvements, was in direct contact with the substrate therefore good adhesion was essential. The high deposition rates, large area depositions, and the maintenance of the stoichiometric composition [8, 9, 10] of the targets were also of high importance.

4.2 Physics of DC-Magnetron Sputtering Deposition System

DC-magnetron sputtering deposition system had the unique advantages compared to other systems of depositions in the research; therefore its choice was easy. However, its operation is not that easy to comprehend at first glance. This method of deposition is a glow-discharge process [9], and it is a plasma polymerization-assisted vapor deposition method [8]. Sputtering is a basic and widely used glow-discharge process. It is an etching process that is used also for surface cleaning and pattern delineation therefore expanding the domain of viable applications [11]. Sputtering is achieved by means of plasma that generate energetic particles that erode a material (target) and deposit the eroded material on the substrate; kind of an atomic sandblasting [8]. These particles are

accelerated towards the substrate by means of an electric field. This technology also uses magnets, as the name implies, that create static magnetic fields parallel to the cathode surface (target) and perpendicular to the electric fields, illustrated in figure 4.1, which are directed from the cathode (target) to the anode (substrate). Here the terminology gets a little confusing but simply stated target means the material used for extraction of surface atoms to be deposited onto the substrate, which is the surface receiving the extracted atoms.

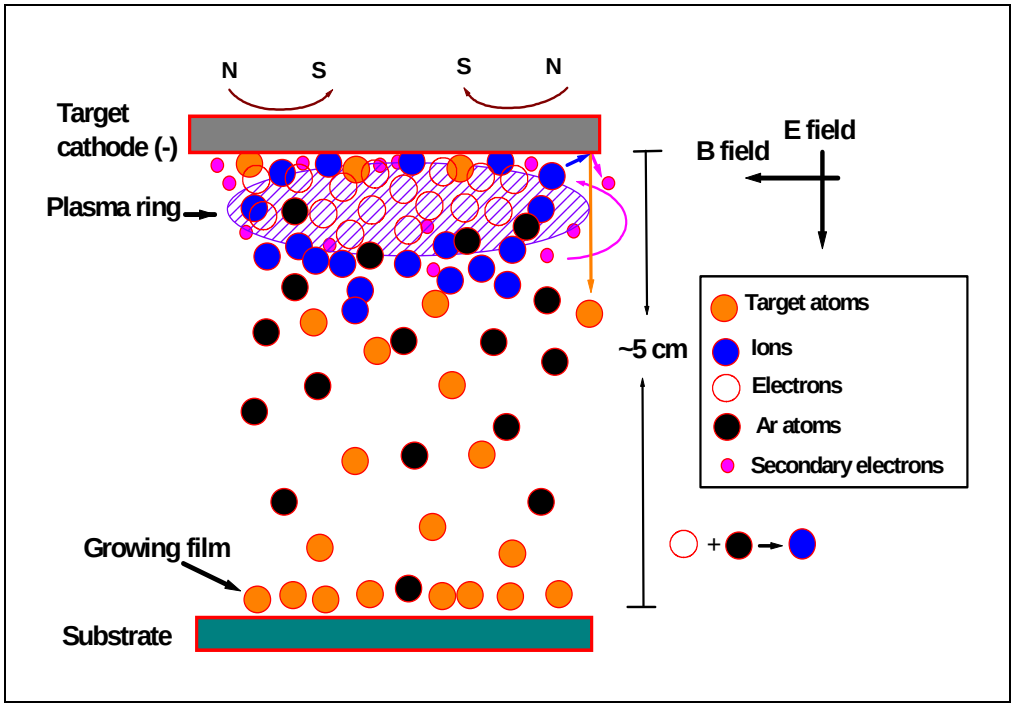

***Figure 4.1*:** Schematic of the physics underlying the DC-sputtering magnetron device. [by Paul Amitesh, IFF]

The transverse magnetic field produces an important effect: the electron trajectories are cycloids near the target. This yields two key advantages compared to other deposition methods: the electrons emitted from target are trapped in the magnetic field close to the target itself and because of this, also the ions are trapped close to the cathode. The electrons are pushed by the magnetic field away transversely. Electron-electron collisions and electron-gas atom (argon) collisions will even enhance this effect and the electrons are trapped to what is called the *etch track* or simply plasma [9]. The plasma gets even denser with electron colliding even with the target itself. Moreover, the plasma particles do not heat the substrate, which could disturb the uniformity of the deposited film that consists of target atoms. A detailed schematic of the vacuum chamber is shown in figure 4.2. Surface atoms from the target material are ejected by incident ions (usually inert gases such as Ar^{+}). The atoms that are actually ejected are called sputtered atoms and they are the ones deposited on the substrate. The atomic collisions that take place on the surface of the target (cathode) during the DC-magnetron sputtering deposition is shown in figure 4.3.

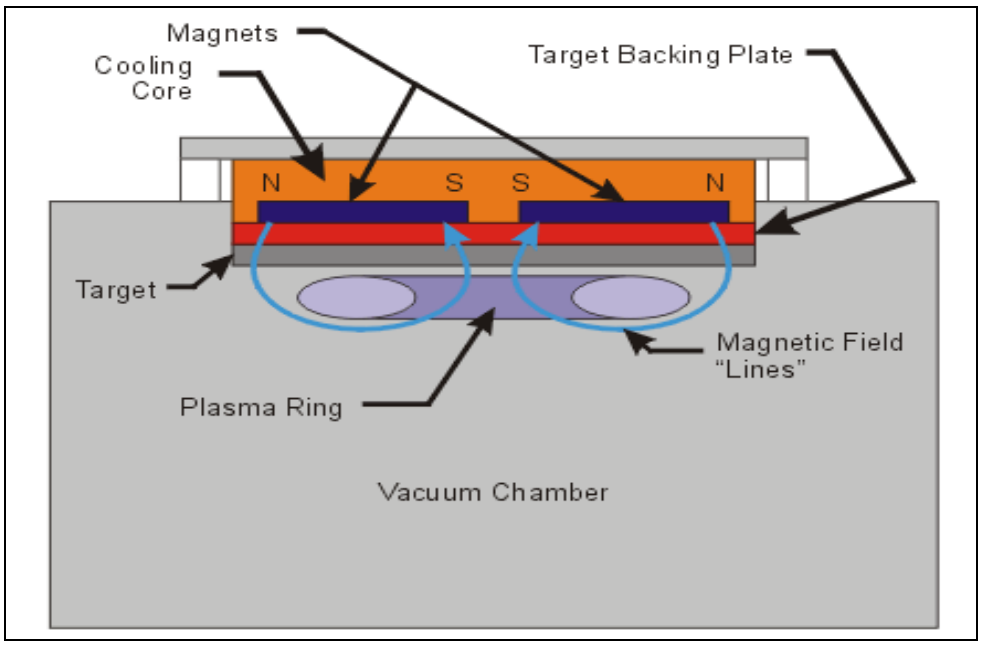

***Figure 4.2*:** Detailed Schematic of the DC-magnetron sputtering process.
[Kindly provided by Hongmei Luo in Chemical Engineering, Tulane University]

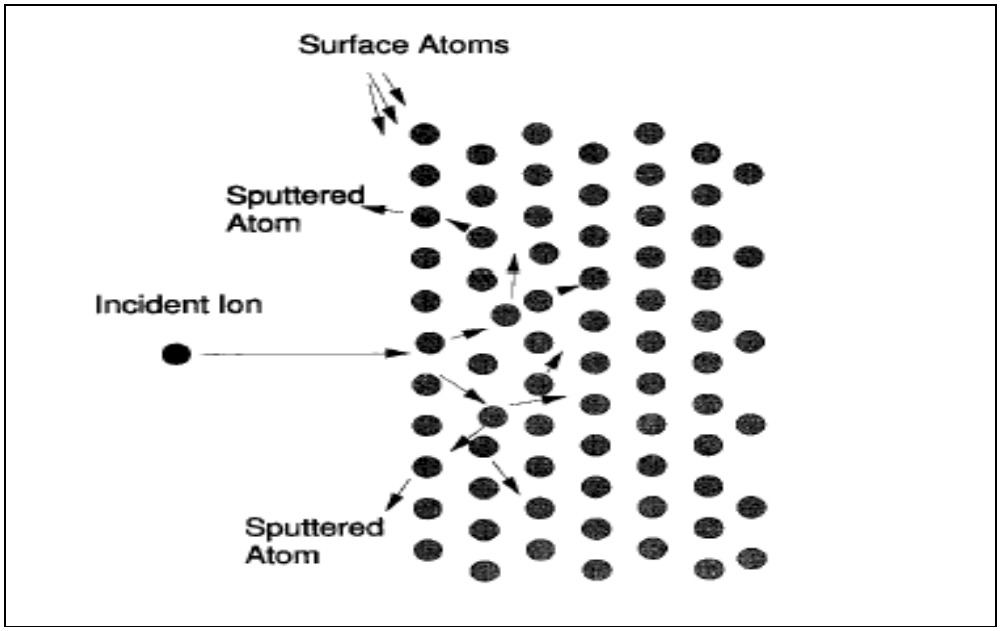

***Figure 4.3*:** Schematic of the Sputtering process. Note that only the surface atoms are sputtered. [8]

4.3 Important Parameters

Several parameters during any deposition have to be determined and followed closely. The base pressure is probably one of the most important parameter. During our depositions, we achieved pressures of 1.0×10^{-7} torr, which is considered high vacuum. The pressure was further reduced by introducing liquid nitrogen (N_2) into a special cylinder in direct contact with the vacuum chamber. The result was a lower pressure (0.8×10^{-7} torr). The chamber was heated a few times to achieve such pressures with external flat-wire type heater element. The Ar pressure was adjusted to 3.2 mtorr by setting the main gate valve to position 287 in respect to 1000 setting (fully opened). The flow of Ar was set by a rotary dial to 38.6 scc/m (standard cubic centimeters per minute). Argon flow is one of the most important parameters in controlling the growth and properties of the deposited films [8]. Other important parameters were the current and voltage of the target. This changed for each type of target used. Since we were using a four-gun sputtering apparatus, we had preloaded film programs with all the required parameters. The computer of the deposition apparatus chose the best voltage and current settings for each gun based on deposition rate, target type, tooling ratio (the actual over the preset deposited film thickness), and the crystal feedback used for thickness monitoring. The voltage and current settings for cobalt were 137 Volts and 0.22 Amps respectively as determined by the computer. For copper, 149

Volts and 0.24 Amps were set for voltage and current respectively. However for iron, the settings were manually adjusted to 153 Volts and 0.40 Amps since there was no crystal present to monitor the thickness of this target. It has to be noted here that all the above values were average values used and there were minor fluctuations during different depositions. This was because the targets oxidized every time the chamber was opened, and a burn out time was required for each target before each deposition for about 3-5 minutes in order to eliminate these contaminations. Since iron had to be set manually, the deposition rate was determined by depositing a thick film (500 nm) on a flat silicon (Si) 2-inch diameter wafer and then taking measurements of the thickness of the film with the profilometer DekTaK IIA manufactured by Sloan which is also placed inside the Thin Films lab. Moreover, the calibration of the tooling ratio of the cobalt and copper were also measure by the above-mentioned profilometer. For more careful studies, the calibration wafers of iron, cobalt, and copper were also examined with the atomic force microscope (AFM) that was used to examine the substrates as mentioned in chapter 3. The results of the DekTak IIA profilometer and the AFM surface analyzer mode yielded the same results of film thicknesses. Actually, there was a minor difference of few Å but this is in the order of the DekTak IIA apparatus "noise" or commonly known as the limitations of the profilometer. Therefore, the difference was acceptable for our measurements. Since the surface

topological examinations showed the structure essential for the requirements of our project, we consequently proceeded with the actual deposition of the multilayers.

4.4 Multilayer Deposition

The films deposited were cobalt and copper multilayers since they have been extensively researched in previous projects. Their good match of their electronic band structures has yielded large magnetoresistance changes [12].

***Figure 4.4*:** Picture of the DC-Sputtering deposition system with the author during an actual deposition.

Once the target materials were chosen, the film thickness had to be determined. Previous research [15, 16] had shown large GMR values (as high as 110%) with copper thickness in the order of few nanometers. Therefore, the spacer (Cu) of our samples was in the range of 2.2 nm to 9.0 nm. Investigating figure 2.6, we can clearly see that our choice of the range of the spacer is fully justified. We are mainly covering the second and third peaks of the graph. There the GMR effect has its maximum value (about 2.2 nm for second peak and 3.8 nm for third peak). Of course, these results are valid only for flat Si surfaces but we were expecting an overall increase to the GMR values due to the geometry of our surfaces. Furthermore, we chose to use two different thicknesses for the magnetic layers of cobalt. The first cobalt thickness was 1.5 nm and the second was 2.5 nm resulting in a 4 layers of magnetic and non-magnetic materials. We decided to deposit two different cobalt thicknesses because there is not exchange coupling between magnetic layers for spacer thickness of about 4.0 nm and larger. The energies required to align the magnetic layers in the antiparallel configuration is different and allows for reversal of the two layers at different magnetic fields. The number of repetitions was determined to be 15, which would make the number of layers of magnetic material a desirable 30 layers of cobalt and 30 layers of copper. Therefore, the total number of the layers is 61 and the total thickness of the structure in the range of 134 nm to 308 nm depending in the thickness of the copper. With

that many layers and the appropriate spacer thicknesses, we should be able to see a respectable GMR effect. As a matter of fact, investigating figure 2.6 we can clearly see that for flat Si substrates the GMR value is about 10-15% for a thickness of spacer (Cu) is 3.8 nm. However, we should stretch the fact that the structure from Leeds University in figure 2.6 is not the exact structure we have deposited. The Co layers have a single thickness of 11 Å (i.e. {Co(11 Å)/ Cu(t_{cu} Å)}x50) whereas our structure has the following configuration:

$$Fe(8.0nm) + \{Cu(t_{Cu}nm) / Co(1.5nm) / Cu(t_{Cu}nm) / Co(2.5nm)\}x15.$$

We have changed the thickness of cobalt (twice) and the total number of multilayers. However, the results should be comparable to each other because the spacer thicknesses (one of the most important variable) are comparable to each other. The spacer thickness (t_{Cu}) is a variable and the iron seed layer only appears on the first block of the 15 deposited. All the structures were duplicated on flat Si wafers for direct comparison. A representation of the first five layers, which are repeated for 15 times, is shown in figure 4.5.

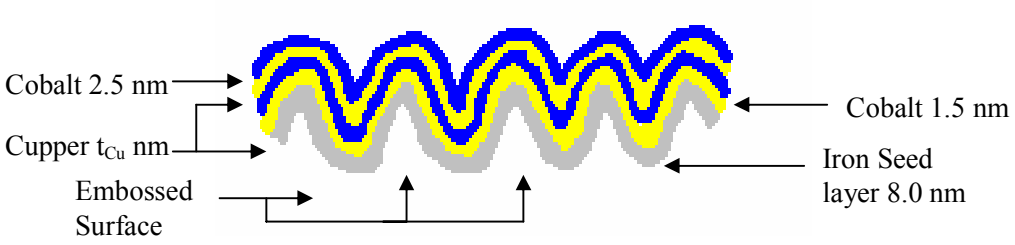

***Figure 4.5*:** Schematic representation of the multilayered structure deposited on embossed surface.

CHAPTER 5

Measurements

5.1 PPMS

After all depositions were made, it was time to measure the properties of the deposited samples. The system chosen for the actual measurements was a physical properties measurement system (PPMS) manufactured by Quantum Design. The specific machine used was Model 6000 PPMS controller. This specific model allows for variable temperature and field measurements. The temperature range of 1.9 K to 400 K yields also temperature dependence of the GMR effect. The cooling of the PPMS was via liquid helium introduced into an annular region called the cooling annulus (shown in figure 5.1) with the assistance of a vacuum pump. The temperature of the helium is then controlled by heaters and thermometers for precise adjustments resulting in accurate temperature control by eliminating temperature gradients. The magnetic field can be set from 7 T to 16 T for longitudinal configuration and 7 T for transverse alignment of the sample. DC resistivity option of the system allows for four-wire or van der Pauw probing of the samples for up to three samples at a time. The current range form the system is from 5 nA to 5 mA and 20 nV sensitivity (see appendix B for explanation of units). The overall accuracy of the

system is 1% from zero up to full field of 16 T and it has 0.2% stability for all temperature ranges. Furthermore, the system allows for horizontal and vertical rotators where the puck (sample holder) is mounted for flexibility with respect to the alignment of the magnetic field with the sample.[1]

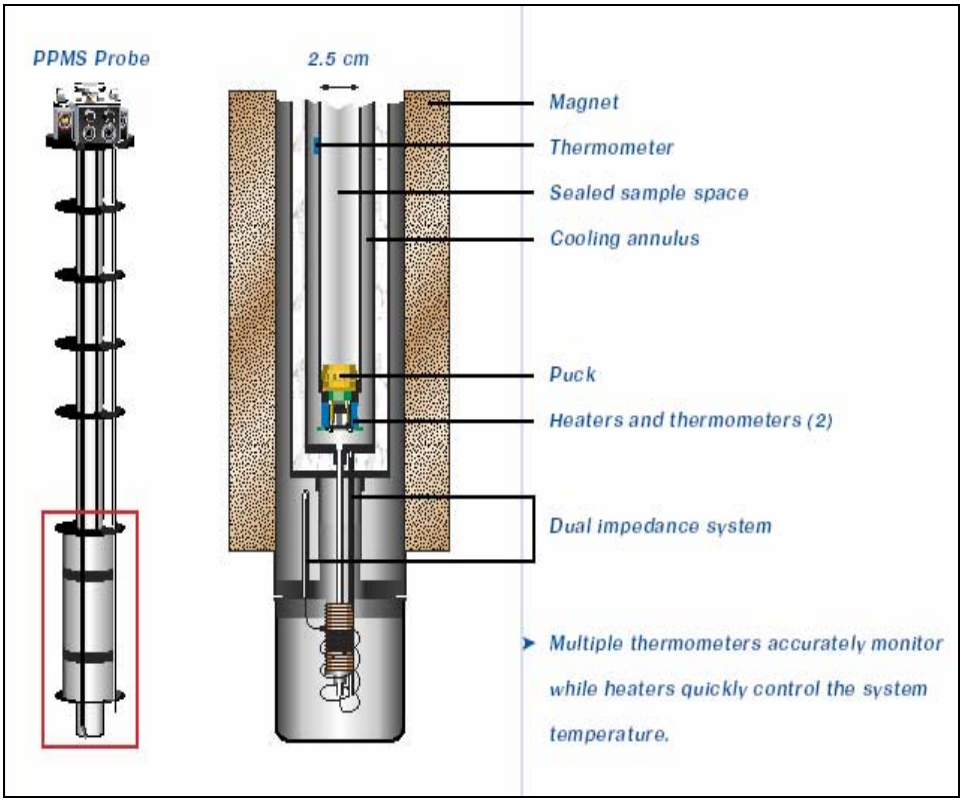

***Figure 5.1*:** Cutout diagram of PPMS 6000 by Quantum Design. [Copyright Quantum Design].

Footnote 1: All the information about PPMS 6000 by Quantum Design was extracted by the company's website and specifically from: *http://www.qdusa.com/products/ppms.html*.

5.2 Parameters Used

Most of our measurements were made at two temperatures: 300 K and 5.0 K. Since a lot of research in GMR sensing was done at 4.2 K (or around that temperature), our choice was justified for comparative reasons. The choice of 300 K (room temperature) was another logical choice since most of GMR sensors in hard drives of PC systems operate at room temperature. The magnetic field was chosen to be parallel to the plane of the substrate since this is the configuration the GMR sensors operate at the vast majority. We started with zero field as the reference point and proceeded to most of the times up to 20 kOe in each direction (parallel and anti-parallel). The time required for such measurements was several hours sometimes with the PPMS running overnight. It should be noted here that not all measurements were successful since cooling down the samples to 4.2 K often damaged the contacts due to internal stresses. Electrical shorts then would allow the current to run outside the deposited film resulting in diminished GMR effect. Conducting carbon tape was used with no success where silver epoxy or silver paste used for electrical contact and mechanical support yielded satisfactory results. Furthermore, attaching the leads or contacts on the sample was probably one of the most difficult tasks since our samples were very thin and thus subject to cracks and mechanical failures from handling them.

5.3 Four Point Probe Method

Most of the resistivity measurements in semiconductor and solid-state science are achieved with the four-point probe method. It has been established since the early 1960s [25] especially for Si wafers but the generic method is used for all samples. This method involves four equally spaced contacts with the sample, the two outer ones being the current probes and the inner ones the voltage probes, as illustrated in figure 5.2. The probe array is assumed to be at the middle of the sample and in a collinear fashion. The reason for the two extra probes in the middle (the voltage probes) is that the contact resistance, which can be significant, is eliminated from the actual sample resistance as long as the sample and contact resistances are small compared to the effective resistance of the measuring device. The resistivity then is described by the following equation developed by Uhlir [26, 27]:

$$\rho = \frac{\pi * w}{\ln 2} * \frac{\Delta V}{I} \quad (5.1).$$

Here ΔV is the voltage across the inner probes, I the current that flows through the outer probes and w is the width of the film. The PPMS system then converted this resistivity to resistance and that was the actual data analyzed to reach the appropriate conclusions.

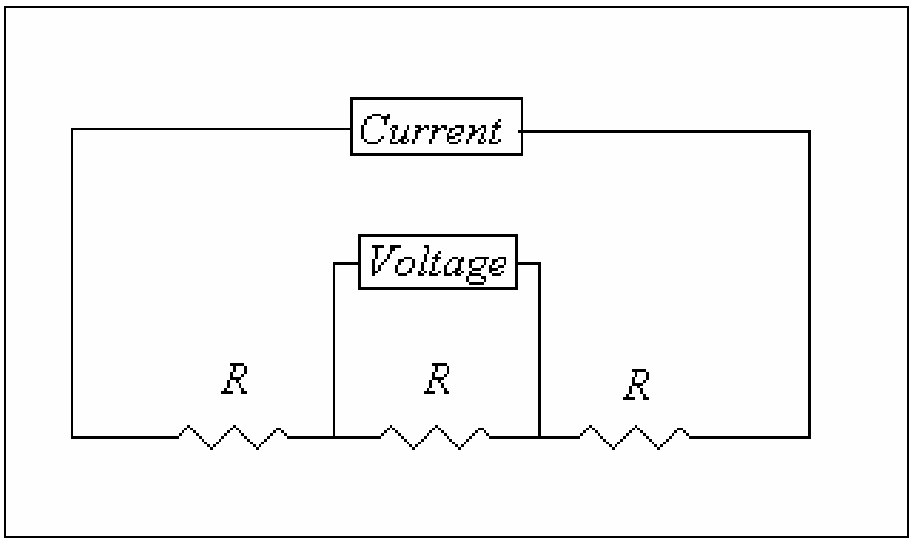

***Figure 5.2*:** Schematic of the four-point probe system.

5.4 Data

When data was extracted from the PPMS computer and it was analyzed using Microsoft Excel® or Origin® 6.0, we were delighted with the results. All of the successful measurements of films grown on the embossed surface were yielding GMR vales higher than the corresponding films grown on Si wafers. Since the depositions of the corresponding embossed and flat silicon surfaces were identical and their measurements during the same actual probing with PPMS, we had results (embossed) with benchmarked values (silicon) to compare to. The comparison of data showed that our initial intuition of GMR enhancement by using embossed substrates was correct. The varied deposited spacer thicknesses for a range of copper produced higher GMR effect compared to the corresponding Si

substrate structures. Data ranging form spacer thickness of 2.2 nm to 8.0 nm has been analyzed and the results are plotted in the nest few figures. The two curves of GMR values compared to each other are shown in figure 5.3. This data set is for the following structure: Fe(8nm)+{Co(1.5nm)/Cu(2.2nm)/Co(2.5nm)/Cu(2.2nm)}x15. The spacer thickness was 2.2 nm (or 22 Å) and the measurements were taken at 10 K. The GMR value for the structure with the flat silicon substrate was 3.1% where the corresponding GMR value for the exact value same structure but with the embossed substrate was on the order of 9.5%. This was a 206% net GMR increase, a 3-fold increase of the effect.

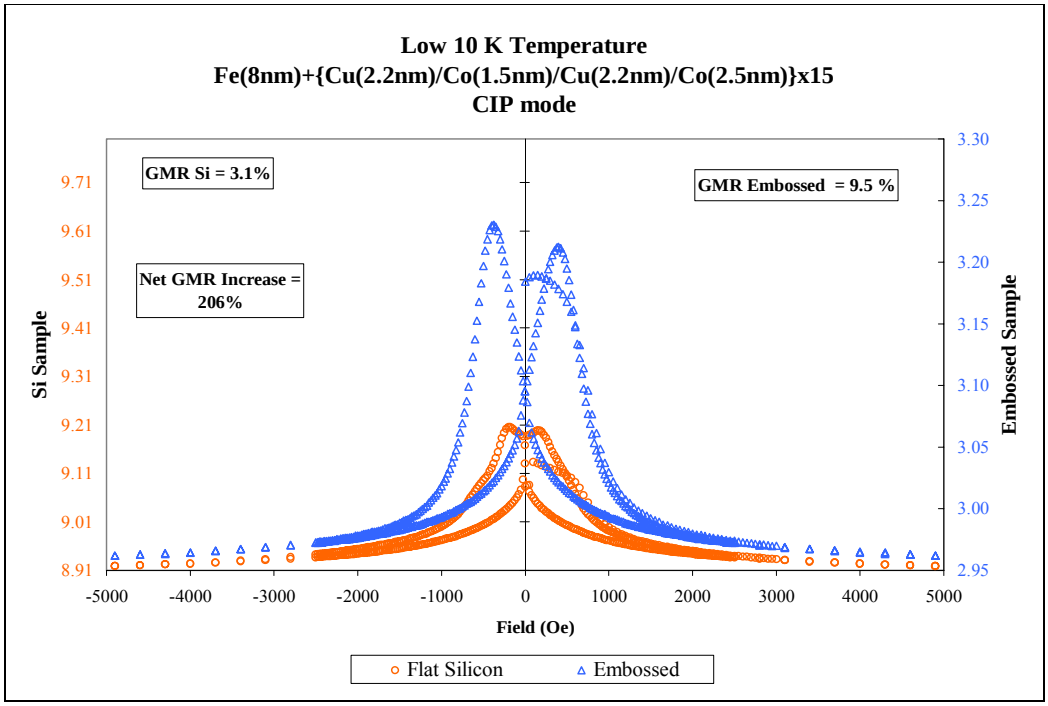

***Figure 5.3*:** Graphical comparison between embossed substrate (triangles) and flat silicon substrate structures for spacer thickness of 2.2 nm at low temperature. Si corresponds to left y-axis and embossed to the right y-axis.

The next logical step is to try to verify our success with different thickness of copper. A thickness of 2.6 nm for the spacer was decided. The structure Fe(8nm)+{Co(1.5nm)/Cu(2.6nm)/Co(2.5nm)/Cu(2.6nm)}x15 was compared to the corresponding flat silicon and again there was a net GMR increase of 6.7% (figure 5.4). The reason for not achieving a huge increase in the GMR value is that there was ferromagnetic coupling between the magnetic layers. Graphically, this would look like the results shown in figure 2.6, that we are between peaks two and three. Therefore the small GMR increase is well justified.

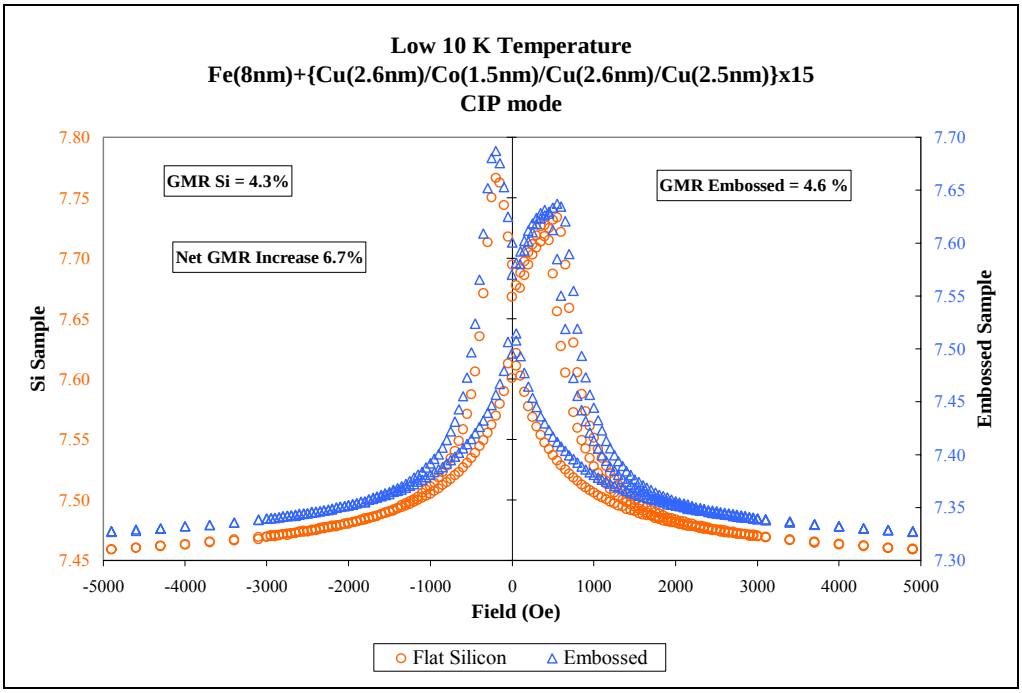

***Figure 5.4*:** Graphical comparison between embossed substrate (triangles) and flat silicon substrate structures for spacer thickness of 2.6 nm at low temperature. Si corresponds to left y-axis and embossed to the right y-axis.

Structures with spacer of 4 nm were also deposited with a net result of an amazing 4-fold increase. The GMR value of the Si wafer came out to be 3.2% (figure 5.5) whereas for the embossed (figure 5.6) the GMR value was 12.2%.

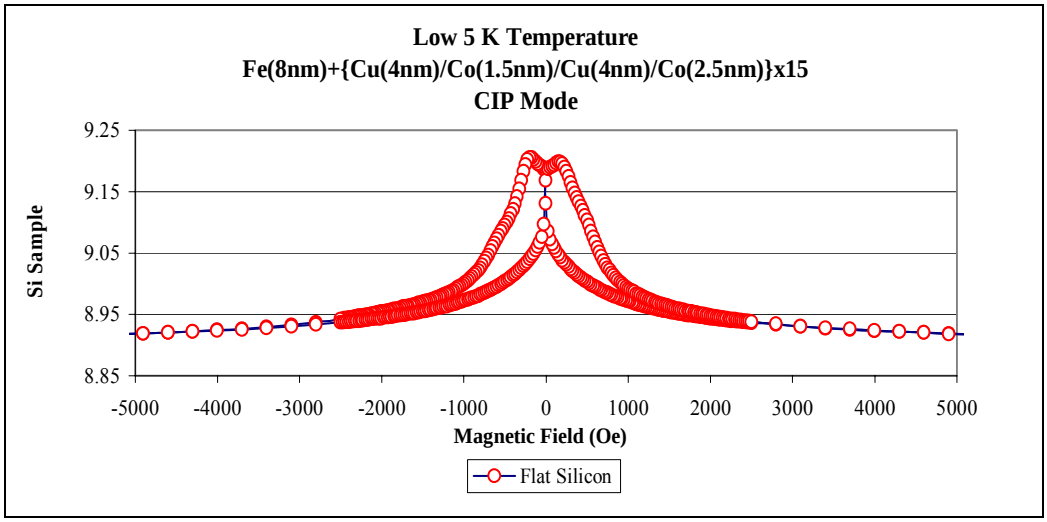

***Figure 5.5*:** Graph of the magnetoresistance curve of flat silicon substrate for spacer thickness of 4.0 nm at low temperature.

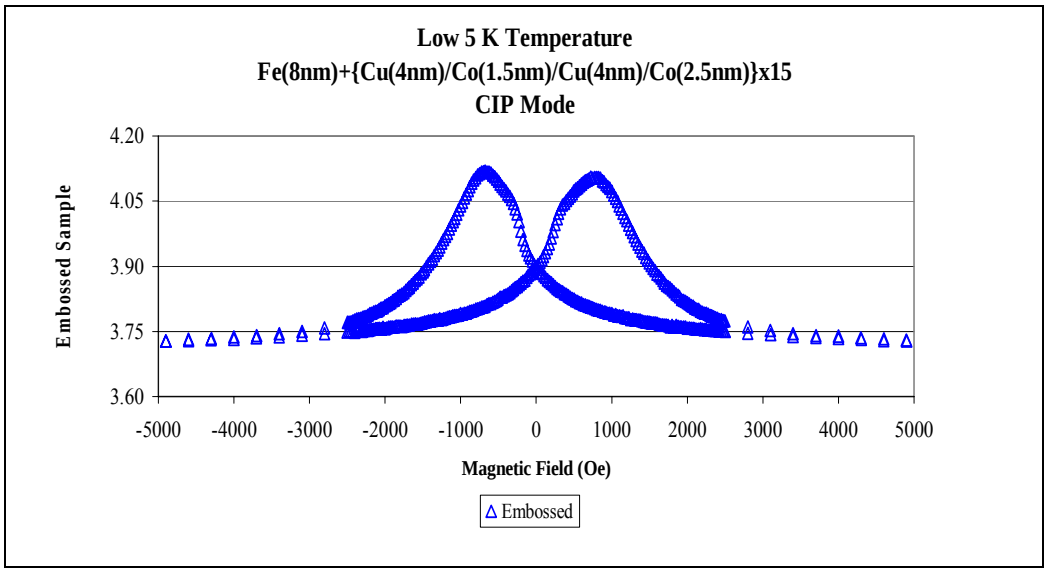

***Figure 5.6*:** Graph of the magnetoresistance curve of embossed substrate for spacer thickness of 4.0 nm at low temperature.

This overall increase of 4 times for GMR value was the maximum increase we got from all samples measured. It was safe to say that our project was a success and that our initial intuition was correct. However, we continued with other samples of different copper thicknesses. Next, we tested structures with spacer thickness of 6.0 nm. Once again, we had successful results. The GMR value for flat silicon substrate was 8.0% and for the embossed surface substrate 11.0% increase, yielding a net increase of 31%, which is depicted in figure 5.7.

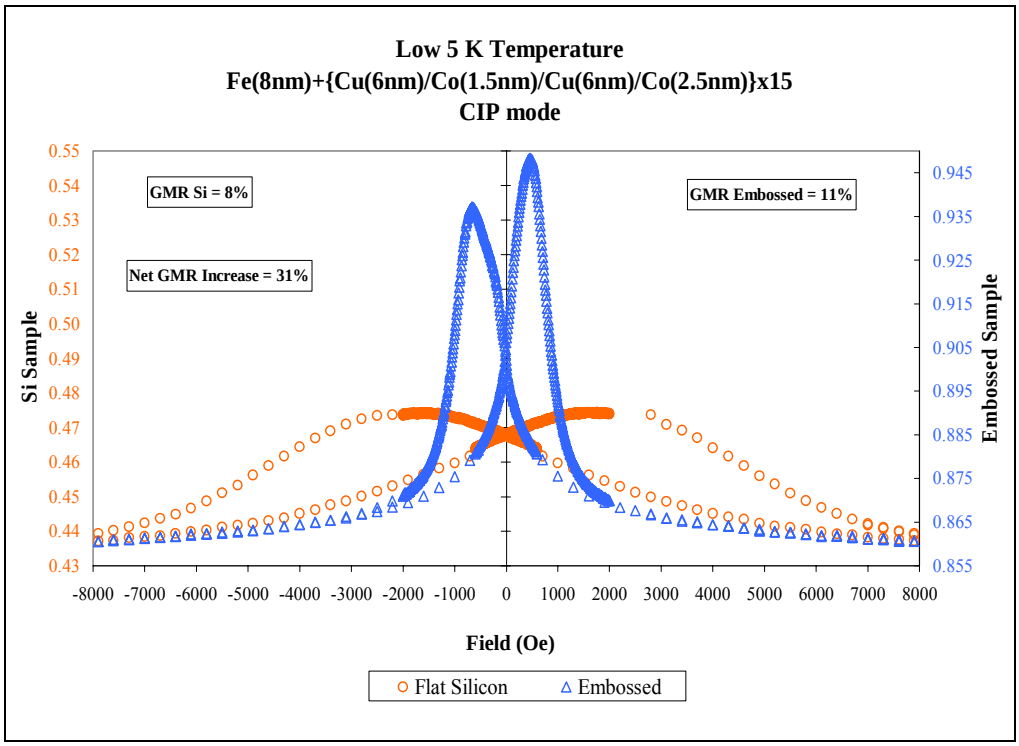

***Figure 5.7*:** Graphical comparison between embossed substrate (triangles) and flat silicon substrate structures for spacer thickness of 6.0 nm at low temperature. Si corresponds to left y-axis and embossed to the right y-axis.

Most data sets had also corresponding room temperature GMR comparison graphs. For instance, the structures with copper spacer of 8.0 nm yielded an overall 22 % for room temperature of 300 K (figure 5.8) where the same structure in low temperature of 5 K was 29% (figure 5.9). The higher value for GMR in lower temperature also agrees with literature that was studied.

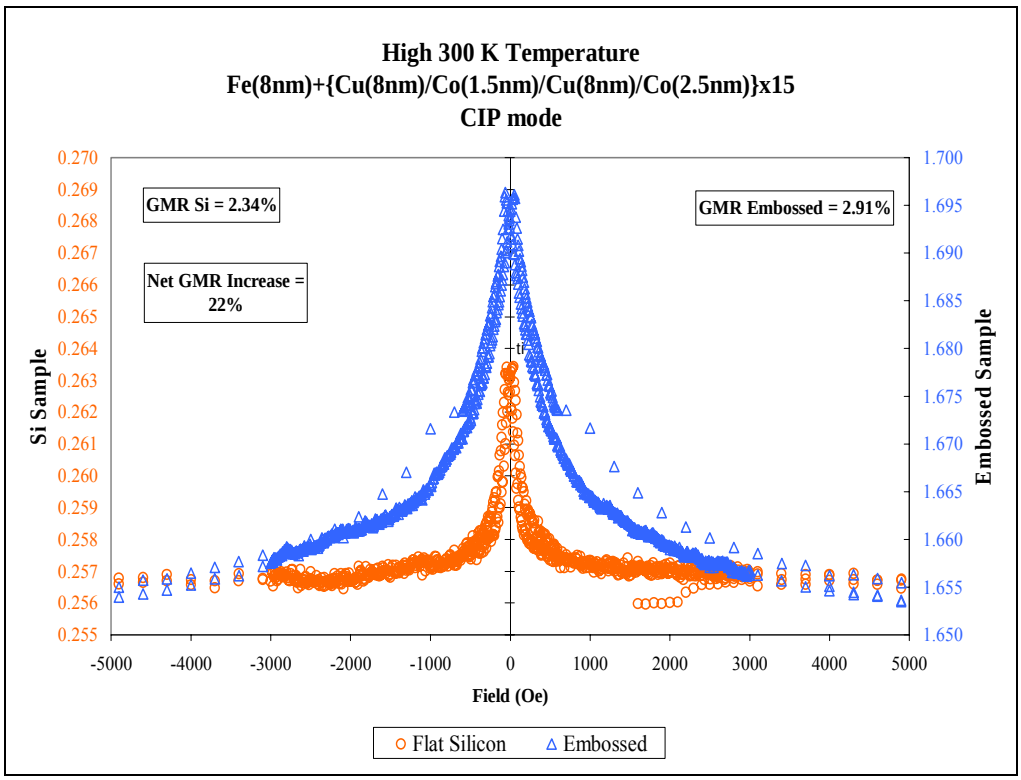

***Figure 5.8*:** Graphical comparison between embossed substrate (triangles) and flat silicon substrate structures for spacer thickness of 8.0 nm at room temperature. Si corresponds to left y-axis and embossed to the right y-axis.

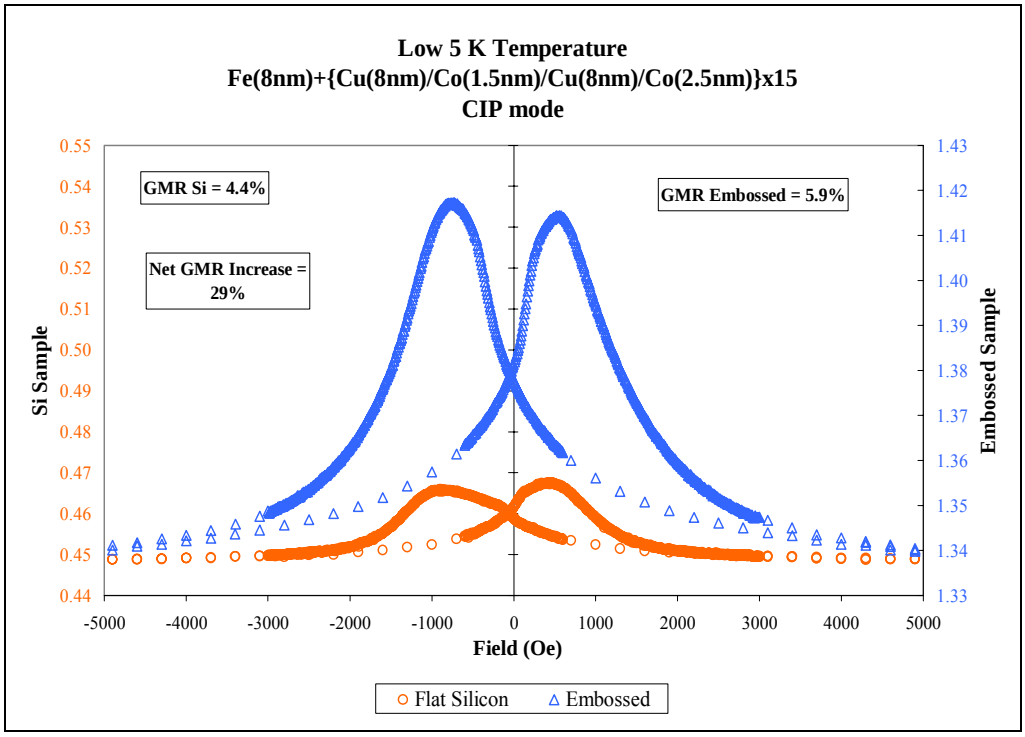

***Figure 5.9*:** Graphical comparison between embossed substrate (triangles) and flat silicon substrate structures for spacer thickness of 8.0 nm at low temperature. Si corresponds to left y-axis and embossed to the right y-axis.

As one can see for the graphs, the GMR net increase was once again respectable using embossed surface compared against the samples with flat silicon substrate. For 8.0 nm spacer the net increase was not a 4-fold but this is justified by observing that the data corresponds to ferromagnetic alignment of the magnetic layers.

Our successful results can be summarized in one graph showing both the flat-silicon substrate data points along with the corresponding embossed surface data points. This graph, shown in figure 5.10, represents most of the work done in this project and it is arguably the most important piece of

this thesis. It clearly indicates the net increase of the GMR effect using embossed surfaces for substrates. It also indicates the range of thickness for the copper spacer where the net increase of the GMR effect is maximum. Moreover, the graph is showing an oscillatory characteristic that is also consistent with previous data for flat silicon substrates. It should be noted that all the measurements of this graph are from low temperature probing.

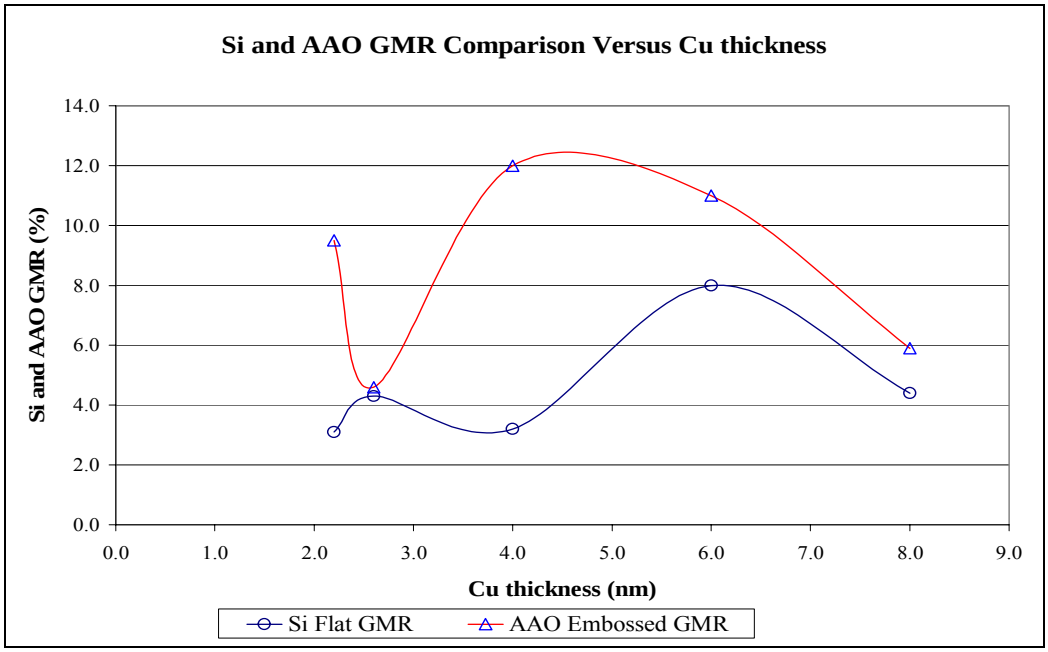

***Figure 5.10*:** Overall comparison of all the successful measurements of embossed surface (Aluminum Oxide AAO) and flat silicon substrates. All measurements at low temperature of 5 K or 10 K.

CHAPTER 6

Conclusion

GMR is arguably one of the most important recent technological achievements of the solid-state physics. The increased sensitivity of GMR sensors, non-volatile applications, and increased data storage as a result of the GMR effect have contributed to an enormous expansion of its applications of the electronic industry in the last 15 years. Scientists and engineers would not probably stop there, though. The applicability and deeper understanding of this phenomenon will continue to affect this industrial aspect for many years to come.

Anodized alumina substrates (AAO) or embossed surfaces as they have been called in this thesis can be successfully [28, 29] used for GMR structures with extraordinary performances. There was a net increase of the GMR effect throughout the range of the thickness of the spacer with a maximum enhancement of 4-fold for 4.0 nm copper spacer.

The underlying reason for these large GMR increases is that the current travels thru the spacer in a combination of both CIP and CPP modes. The mode called CAP [7, 20, 21, 22, 23, 28, 29] where previous studies and this project have shown that magnetic sensing can be further improved by a simple but elegant choice of novel substrates.

Such an improvement of the GMR effect can have a great impact on the industrial technology sector. Most of today's hard disk drives utilize GMR sensors in order to read the data (figure 2.16, IBM). Therefore, a more sensitive GMR sensor translates into more dense hard drives and thus less expensive computers. MRAM is another choice of the list of applications. The GMR effect can be utilized to manufacture non-volatile memories and our structures with embossed substrates can even enhance the result. Metal detection, navigation, and low-magnetic field sensing are major candidates for our structures.

The inexpensive manufacture costs of the embossed substrates and relatively easiness of the deposition of the structures along with the mass production advantage of them, almost guarantees that the industry will take gain of the benefits of embossed GMR structures.

SUPPORT

This work was partially supported by DARPA grant MDA972-02-1-0001 and NSF grant EPS 0092001. The author is greatly thankful to these organizations for their grants that made this work possible.

REFERENCES

[1] Waser, Rainer (Ed), *Nanoelectronics and Information Techlology: Advanced Electronic Materials and Novel Devices* Weinheim*:* Wiley-VCH, 2003.

[2] M. N. Baibich, J. M. Broto, A. Fert, N. Nguyen van Dau, F. Petroff, P.Etienne, G. Crauzet, A. Friedrich, and J. Chazelas, *Phys. Rev. Lett*. **61,** 2472 (1988).

[3] Robert C. O'Handley, *Modern Magnetic Materials: Principles and Applications* New York: John Wiley & Sons, 2000.

[4] Uwe Hartmann (Ed.), *Magnetic Multilayers and Giant Magnetoresistance* Berlin: Springer 2000.

[5] S. S. P. Parkin, N. More, and K. P. Roche, *Phys. Rev. Lett*. **64,** 2304, (1990).

[6] A. E. Berkowitz, J. R. Mitchell, M. J. Carey, A. P. Young, D. Rao, A. Starr, S. Zhang, F. E. Spada, F. T. Parker, A. Hutten, and G. Thomas, *J. Appl. Phys.* **73,** 5320, (1993).

[7] M. A. M. Gijs, M. T. Johnson, A. Reinders, P. E. Huismann, R. J. M. van de Veerdonk, S. K. J. Lenczowski, R.M.J. van Gansewinkel, "Perpendicular giant magnetoresistance of Co/Cu multilayers

deposited under an angle on grooved substrates", *Appl. Phys. Lett.,* vol. **66**, pp. 1839-41, 1995.

[8] K. Seshan (Ed), *Handbook of Thin-Film Deposition and Techniques-Principles, Methods, Equipment and Applications,* 2nd Edition, New Jersey: Noyes/William Andrew Publishing, 2002.

[9] R. F. Bunshah (Ed), *Handbook of Deposition Technologies for Films and Coatings-Science, Technology and Applications,* 2nd Edition, New Jersey: Noyes/ William Andrew Publishing, 1994.

[10] R. F. Bunshah (Ed), *Deposition Technologies for Films and Coatings: Developments and Aplications* New Jersey: Noyes, 1982.

[11] Thornton, J. A., *Metal Finishing,* 77:45, 1979.

[12] J. M. MacLaren, X. G. Zhang, W. H. Butler, X. Wang, *Phys. Rev. B,* **590,** (1999) 5470-7548.

[13] A. E. Berkowitz, J. J. R. Mitchell, M. J. Carey, A. P. Young, S. Zhang, F. E. Spada, F. T. Parker, H. Hutten, G. Thomas, *Phys. Rev. Lett.,* **68,** no. 25 (1992) 3745.

[14] R. E. Camley, J. Barnas, *Phys. Rev. Lett.,* **63,** (1989) 2472.

[15] S. S. P. Parkin, Z. G. li, and D. J. Smith, "Giant magnetoresistance in Antiferromagnetic Co/Cu Multilayers," *Appl. Phys. Lett.,* **58,** 2710 (1991).

[16] S. S. P. Parkin, R. Bhadra, and K. P. Roche, "Oscillatory Magnetic Excange Coupling Through Thin Copper Layers," *Phys. Rev. Lett.,* **66,** 2152 (1991).

[17] Dieny, B., V. Speriosu, S. S. P. Parkin, B. A. Gurney, D. R. Wilhoit, and D. Mauri, *Phys. Rev. B,* **43**, 1297 (1991a).

[18] Dieny, B., V. Speriosu, S. S. P. Parkin, B. A. Gurney, P. Baumgart, and D. R. Wilhoit, *J. Appl. Phys.,* **69,** 4774 (1991b).

[19] J. Bass, W. P. Pratt Jr., *J. Magn. Magn. Mater.,* **200,** (1999) 247.

[20] M. A. M. Gijs, S. K. J. Lenczowski, J. B Giesbers, R. J. M. van de Veerdonk, M. T. Johnson, R. E. Jungblut, A. Reinders, R.M.J. van Gansewinkel, *J. Magn. Magn. Mater.,* **151**, (1995) 333.

[21] G. R. Harp, S. S. P. Parkin, R. F. C. Farrow, R. F. Marks, M. F. Toney, Q. H. Lam, T. A. Rabedeau, R. J. Savoy, *Phys. Rev. B.,* **47,** (1993) 8721.

[22] T. Ono, T. Shinjo, *J. Pjys. Se. Jpn.,* **64,** (2) (1995) 363.

[23] T. Shinjo, T. Ono, *J. Magn. Magn. Mater.,***77,** (1998) 31.

[24]P. M. Levy, S. Zhang, T. Ono, T. Shinjo, "Electrical Transport in Corrugated Multilayered Structures," **52,** (1995) 16049.

[25] Hargreaves, J. K., and Millard, D., *Brit. J. Phys.,* **13,** (1962) 231-234.

[26] Uhlir, A., *Bell Syst. Tech. J.,* **34,** (1955) 105-128.

[27] R. Hall, *J. Sci. Instrum.,* **44,** No 1 (January 1967) 53-54.

[28] Athanasios Chalastaras, Leszek M. Malkinski, Jin-Seung Jung, Seung-Lim Oh, Jin-Kyu Lee, Carl A. Ventrice, Jr., Vlodymyr Golub, and Gleander Taylor, "*GMR Multilayers on a New Embossed Surface*", accepted for publication to IEEE Transactions on Magnetics.

[29] Leszek M. Malkinski, Athanasios Chalastaras, A. Vovk, Jin-Seung Jung, Seung-Lim Oh, Jin-Kyu Lee, and Carl A. Ventrice, Jr, "Magnetoresistive Multilayers Deposited on the AAO Mebranes", accepted for publication to *Journal of Magnetism and Magnetic Materials*.

APPENDIX A

List of Acronyms

GMR ..... Giant magnetoresistance

MR ..... magnetoresistance

AFM ..... Atomic Force Microscope

SEM ..... Scanning Electron Microscope

DC ..... Direct Current

PPMS ..... Physical Properties Measurement System

MOKE ..... Magneto Optical Kerr Effect

MRAM ..... Magnetoresistive Random Access Memory

PC ..... Personal Computer

CIP ..... Current Into the Plane

CPP ..... Current Perpendicular to the Plane

CAP ..... Current at an Angle to the Plane

NSF ..... National Science Foundation

DARPA ..... Defense Advanced Research Projects Agency

AMRI ..... Advanced Materials Research Institute

UNO ..... University of New Orleans

APPENDIX B

List of Units Used

K.....Kelvin

nm.....nanometer

Å.....Angstrom

mtorr..... millitorr

T .....Tesla

mA..... milliAmpere

nA.....nanoAmpere

nV.....nanoVolt

kOe.....kiloOersted

π.....pi, 3.14

ln.....natural logarithm

APPENDIX C

Publications by the Author on the Subject

Athanasios Chalastaras, Leszek M. Malkinski, Jin-Seung Jung, Seung-Lim Oh, Jin-Kyu Lee, Carl A. Ventrice, Jr., Vlodymyr Golub, and Gleander Taylor, "GMR Multilayers on a New Embossed Surface", accepted for publication to *IEEE Transactions on Magnetics*.

Leszek M. Malkinski, Athanasios Chalastaras, A. Vovk, Jin-Seung Jung, Seung-Lim Oh, Jin-Kyu Lee, and Carl A. Ventrice, Jr, "Magnetoresistive Multilayers Deposited on the AAO Mebranes", accepted for publication to *Journal of Magnetism and Magnetic Materials*.

VITA

Athanasios Chalastaras was born in Chalkida, Greece, in 1974, and lived his young years in Attali, Greece. He received his high school diploma in 1992 from First Technical High School of Chalkida. He then moved to New Orleans, USA in 1994 to further enhance his education. He received a Certificate of Completion in English as A Second Language form Delgado Community College in New Orleans. In 1996, he transferred to University of New Orleans where he completed his undergraduate degree in Naval Architecture and Marine Engineering at the end of 2001. Athanasios further continued to improve his education in Master's Physics at UNO starting in January 2002. Numerous presentations have been given by him and he has won third place in Master's category at Louisiana Conference in Lafayette in 2003. As of August 2003, Athanasios is a Doctor of Philosophy student at Tulane University with theoretical atomic physics concentration.